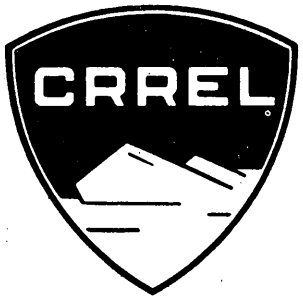

Research Report 120

STRESS AND WAVE PATTERNS IN SOILS SUBJECTED TO DYNAMIC LOADS

by

R. K. Bernhard

MARCH 1967

U.S. ARMY MATERIEL COMMAND
COLD REGIONS RESEARCH & ENGINEERING LABORATORY
HANOVER, NEW HAMPSHIRE

DA Task 1V025001A13001

PREFACE

The work described in this report was performed by Dr. Rudolf K. Bernhard, Expert to USA CRREL for the Applied Research Branch (Mr. A. Wuori, Chief), Experimental Engineering Division (Mr. K. A. Linell, Chief). Mr. F. J. Sanger, Special Assistant, EED, technically reviewed the report.

The report is divided into four parts: Parts I and II cover investigations of the reliability of shear stress measurements in soils subjected to vibratory loads for biaxial and triaxial systems respectively. Part I is a summary only. A more detailed treatment may be found in USA CRREL Technical Report 90. Part III is a study of three-dimensional "principal" stress patterns produced in soil subjected to vibratory loads. Part IV is a theoretical analysis of some aspects of soil wave propagation in stratified soil.

USA CRREL is an Army Materiel Command laboratory

CONTENTS

ILLUSTRATIONS

CONTENTS (Cont'd)

TABLES

SUMMARY

The report is divided into four parts: Parts I and II cover investigations of the reliability of shear stress measurements in soils subjected to vibratory loads for biaxial and triaxial systems, respectively. Part I is a summary only (see USA CRREL Technical Report 90 for detailed treatment). Part III is a study of three-dimensional "principal" stress patterns produced in soil subjected to vibratory loads. Part IV is a theoretical analysis of some aspects of soil wave propagation in stratified soil. From the measurements of five shear stresses and one normal stress, the stress distribution of a triaxial system can be determined. In noncohesive soils triaxial stress fields due to vibratory loads can be determined by recording six independent stress components. Sinusoidal force excitation and impact excitation yield time-distance graphs which can be used to determine reflection and refraction techniques in stratified soils.

STRESS AND WAVE PATTERNS IN SOILS SUBJECTED TO DYNAMIC LOADS

by

R. K. Bernhard

PART I. TWO-DIMENSIONAL SHEAR STRESS MEASUREMENTS

Vibratory (sinusoidal) loads were generated by a three-mass mechanical oscillator* on the surface of the soil and transmitted to miniaturized shear cells (Fig. 1) and pressure cells (diam 0.9 in., height 1.2 in.) buried 6 in. beneath the center of the contact plate (Fig. 2). The pressure cell and oscillator are described in ASTM Technical Publication No. 156. The soil, a predominantly homogeneous and non-cohesive soil (dry beach sand), was confined in a concrete basin 24 ft long, 11 ft wide and 5 ft deep. The results and analysis are given in CRREL Technical Report 90. Comparison between measured values and values computed for a biaxial system showed a standard deviation of 4.75% for shear stresses and 5.22% for normal stresses. From the few pilot experiments it was tentatively concluded that shear and normal stress vectors can be measured in situ provided that the necessary precautions are adhered to, particularly when inserting the cells into the soil.

PART II. THREE-DIMENSIONAL SHEAR STRESS MEASUREMENTS

Introduction

To investigate stress distribution in soils, the determination of as many shear- and normal-stress components as possible is of primary significance since the compatibility of these various parameters will indicate the accuracy of the measuring technique. Only after a reliable measuring technique has been established will it be possible to compare experimental results with theoretical approaches.

Previous studies referring to triaxial systems have been confined to pressure measurements. This investigation supplements previous work by measuring five shear stresses and one normal stress, in order to determine the compatibility of these measured stresses with computed normal stresses.

Measurements

A "dry" non-cohesive soil was used to avoid the numerous ramifications involving friction, viscosity, plasticity, etc., usually connected with a study of cohesive soils. The soil was an almost non-cohesive gravelly sand of approximately 4% moisture content. Instrumentation and measuring techniques were the same as for the biaxial measurements (see Pt. I, also Bernhard, 1961; 1963; and Ahlvin, 1954) except that the cells (6 in. below the surface) were placed at 1 ft horizontal distance from the vertical force vector.

Notation and measuring systems are indicated in Figure A1 (App. A), p. 43.

Any determination of the three principal stresses in a three-dimensional system requires six independent parameters. In this investigation, five shear stresses (τ_{12}, τ_{23}, τ_{31}, τ_{45} and τ_{46}) and one normal stress (σ_1) were measured.

*Consisting of eccentrically supported rotating weights producing a vertical centrifugal force vector.

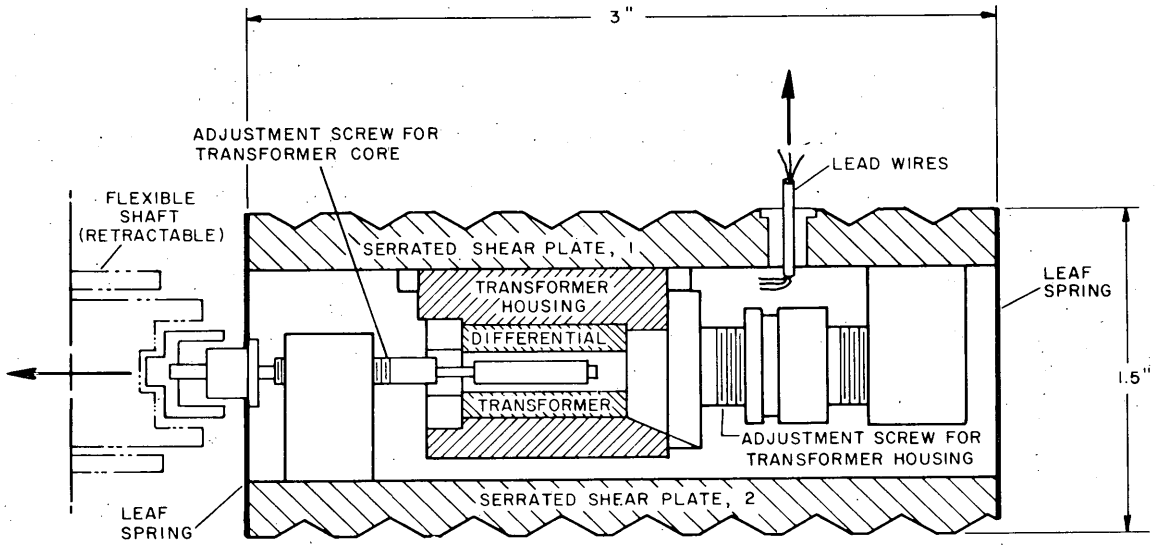

Figure 1. Shear cell (top cover removed).

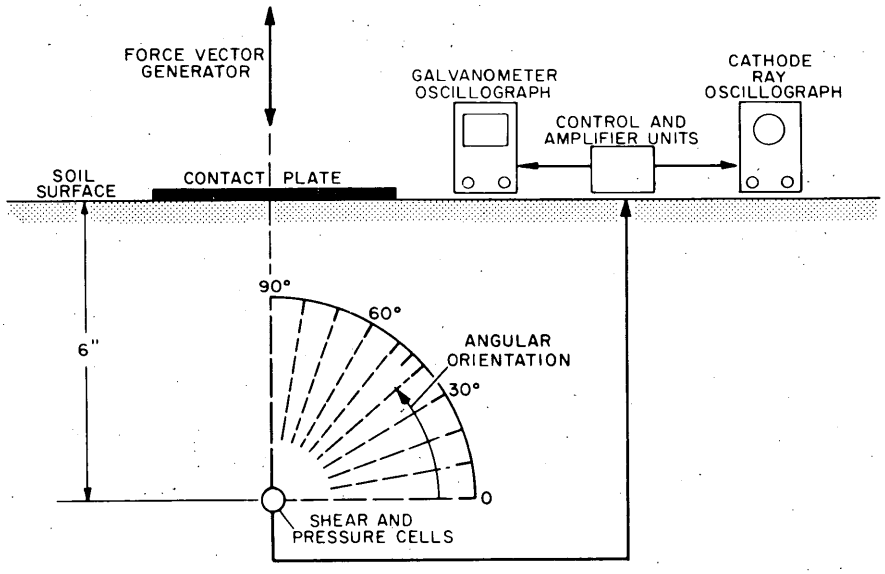

Figure 2. Experimental setup.

Since shear stresses τ_{45}, τ_{46} and τ_{56} are in the same tetrahedral plane, their vector sum must be zero, indicating that for this plane the three shear stresses are not independent. Hence the normal stress σ_1 has been substituted for shear stress τ_{56} as the sixth independent parameter to be measured.

Experimental results

Six series of readings were made under identical conditions for each stress: a vertical force vector of ± 500 lb at 50 cps. In Figure 3 a set of the original time-shear stress records (galvanometer oscillograph images, series 1) for τ_{45}, τ_{31}, τ_{12}, and τ_{23} are reproduced. Table I summarizes the experimental results for the six measured stress vectors.

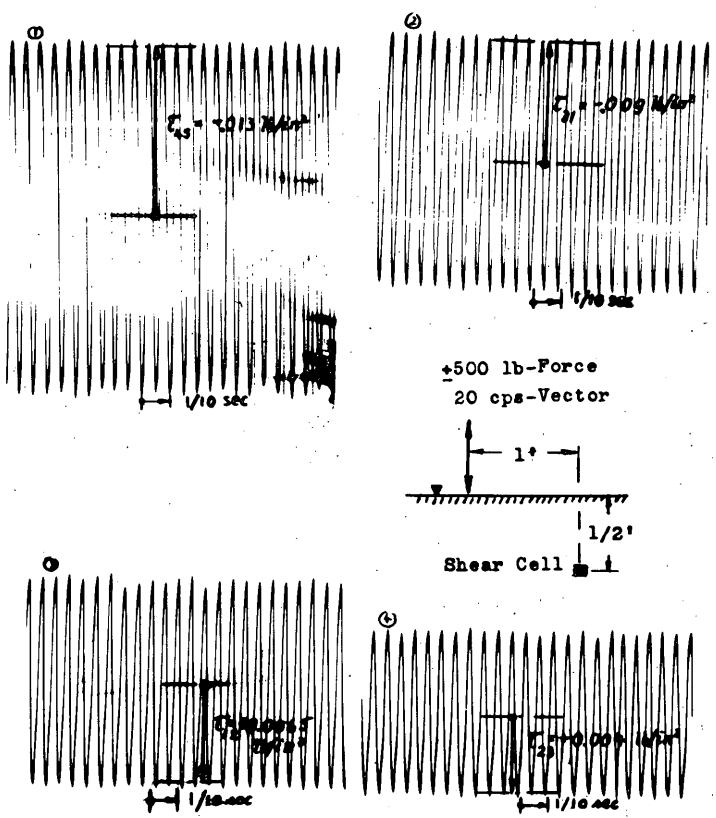

Figure 3. Shear stress-time records (galvanometer oscillograph).

Evaluation

The equations for evaluating the results (App. A) follow the well-known triaxial-stress theory in a half-space continuum of a homogeneous and isotropic elastic medium.

Table I. Measured shear and normal stresses (τ and σ in: 10^{-2}lb/in.^{2}).

Series		1	2	3	4	5	6	Mean
Shear stress:	τ_{12}	0.65	0.35	0.55	0.4	0.6	0.45	0.50
	τ_{23}	0.4	0.1	0.3	0.15	0.35	0.2	0.25
	τ_{31}	-0.9	-1.1	-1.2	-1	-1	-0.8	-1.0
	τ_{45}	-1.3	-1.7	-1.6	-1.45	-1.45	-1.4	-1.5
	τ_{46}	-2.55	-2.45	-2.5	-2.4	-2.6	-2.5	-2.5
Normal stress:	σ_1	+9.2	+8.8	+9.0	+8.9	+9.1	+9.0	+9.0

$\tau_{56} = \tau_{45} + \tau_{46} = -4$ (computed)

Plus sign indicates compression.

The stress computations comprise determination of:

1. The normal stresses σ_1 from the experimentally-obtained shear stresses τ_{ij} $(i \neq j)$
2. The principal stress differences $(s_{i_1} - s_{i_2})$ from eq A 15 (App. A):

$$s_{i_1} - s_{i_2} = \sqrt{(\sigma_{i_1} - \sigma_{i_2})^2 + 4\,\tau_{i_1 i_2}^2}$$

3. The principal stresses from eq A 16:

$$s_{i_1} = \tfrac{1}{3}\sum_{i=1}^{i=3}\sigma + (s_{i_1} - s_{i_3}) + (s_{i_1} - s_{i_2})$$

$$s_{i_2} = s_{i_1} - (s_{i_1} - s_{i_2})$$

$$s_{i_3} = s_{i_1} - (s_{i_1} - s_{i_3})$$

4. The maximum shear stresses from eq A 17:

$$s^s_{i_1 i_2} = \tfrac{1}{2}(s_{i_1} - s_{i_2})$$

5. The direction cosines ℓ_i, m_i, n_i from eq A21:

$$\ell_i = \frac{(s_{i_2} - \sigma_i)(s_{i_3} - \tau_i) + \tau_{ij}^2}{(s_{i_2} - s_{i_1})(s_{i_3} - s_{i_1})}$$

In the following computations for the normal and principal stresses a plus sign indicates compression. All stresses are expressed in 10^{-2} lb/in.^{2}.

Normal stresses. From the measured five shear stresses and one measured normal stress:

$$\sigma_1 = +9 \text{ (measured)}$$
$$\sigma_2 = 2\tau_{46} + \sigma_1 = +4$$
$$\sigma_3 = 2(\tau_{45} + \tau_{46}) + \sigma_1 = +1$$
$$\sigma_4 = \tau_{23} + 1/2\,(\sigma_2 + \sigma_3) = +2.75$$
$$\sigma_5 = \tau_{13} + 1/2\,(\sigma_1 + \sigma_3) = +4$$
$$\sigma_6 = \tau_{12} + 1/2\,(\sigma_1 + \sigma_2) = +7$$
$$\sigma_7 = \sigma_1 + \sigma_2 - \sigma_6 = +6$$
$$\sigma_8 = \sigma_2 + \sigma_3 - \sigma_4 = +2.25$$
$$\sigma_9 = \sigma_1 + \sigma_3 - \sigma_5 = +6\,.$$

Principal stress differences. From eq A 15:

$$s_1 - s_2 = \sqrt{25 + 1} = 5.099$$
$$s_1 - s_3 = \sqrt{64 + 4} = 8.246$$
$$s_2 - s_3 = \sqrt{9 + 0.25} = 3.041\,.$$

Principal stresses. From eq A 16:

$$s_1 = 1/3\,(14 + 8.246 + 5.099) = 9.115$$
$$s_2 = 9.115 - 5.099 = 4.016$$
$$s_3 = 9.115 - 8.246 = \underline{0.869}$$
$$\sum s_i = 14.000 = \sum_{i=1}^{i=3} \sigma = \text{First invariant.}$$

Maximum shear stresses. (s^s_{ij}) from eq A 17:

$$s^s_{12} = 2.5495$$
$$s^s_{13} = 4.123$$
$$s^s_{23} = 1.5205$$

Direction cosines. The determination of direction cosines α, β, and γ follows from eq A 21:

$$\ell_i^2 = \cos^2 \alpha_i = \frac{(s_2 - \sigma_i)(s_3 - \sigma_i) + \tau_{ij}^2}{(s_2 - s_1)(s_3 - s_1)} = \frac{A_i + \tau_{ij}^2}{D}$$

$$m_i^2 = \cos^2 \beta_i = \frac{(s_3 - \sigma_i)(s_1 - \sigma_i) + \tau_{ii}^2}{(s_3 - s_2)(s_1 - s_2)} = \frac{B_i + \tau_i^2}{E}$$

$$n_i^2 = \cos^2 \gamma_i = \frac{(s_1 - \sigma_i)(s_2 - \sigma_i) + \tau_{ii}^2}{(s_1 - s_3)(s_2 - s_3)} = \frac{C_i + \tau_i^2}{F}$$

Denominators (D, E, F).

$D = (-5.099)(-8.246) = +42$

$E = (-3.041)(+5.099) = -15.5$

$F = (+8.246)(+3.041) = +25.2$

Numerators (A_i, B_i, C_i).

$A_1 = (s_2 - \sigma_1)(s_3 - \sigma_1) = (4.016 - 9)(0.869 - 9) = (-4.984)(-8.131) = +40.5$

$A_2 = (s_2 - \sigma_2)(s_3 - \sigma_2) = (4.016 - 4)(0.869 - 4) = (+0.016)(-3.131) = -0.04$

$A_3 = (s_2 - \sigma_3)(s_3 - \sigma_3) = (4.016 - 1)(0.869 - 1) = (+3.016)(-0.131) = -0.395$

$B_1 = (s_3 - \sigma_1)(s_1 - \sigma_1) = (0.869 - 9)(9.115 - 9) = (-8.131)(+0.115) = -0.935$

$B_2 = (s_3 - \sigma_2)(s_1 - \sigma_2) = (0.869 - 4)(9.115 - 4) = (-3.131)(+5.115) = -16.0$

$B_3 = (s_3 - \sigma_3)(s_1 - \sigma_3) = (0.869 - 1)(9.115 - 1) = (-0.131)(+8.115) = -1.062$

$C_1 = (s_1 - \sigma_1)(s_2 - \sigma_1) = (9.115 - 9)(4.016 - 9) = (+0.115)(-4.984) = -0.574$

$C_2 = (s_1 - \sigma_2)(s_2 - \sigma_2) = (9.115 - 4)(4.016 - 4) = (+5.115)(+0.016) = +0.082$

$C_3 = (s_1 - \sigma_3)(s_3 - \sigma_3) = (9.115 - 1)(4.016 - 1) = (+8.115)(+3.016) = +24.42.$

Eq A 21 yields:

$$\ell_1^2 = \frac{A_1 + \tau_{13}^2}{D} = \frac{40.5 + 1}{+42} = 0.975;\ \ell_1 = \cos\alpha_1 = 0.989;\ \alpha_1 = +8°30'$$

$$m_1^2 = \frac{B_1 + \tau_{13}^2}{E} = \frac{-0.935 + 1}{-15.5} = -0.00418;\ m_1 = \cos\beta_1 = 0.0647;\ \beta_1 = +86°42'$$

$$n_1^2 = \frac{C_1 + \tau_{13}^2}{F} = \frac{-0.574 + 1}{+25.2} = +0.0169;\ n_1 = \cos\gamma_1 = 0.13;\ \gamma_1 = -82°30'$$

similarly: $\ell_2 = \cos\alpha_2 = 0.0706;\ \alpha_2 = -85°57'$

$m_2 = \cos\beta_2 = 0.985;\ \beta_2 = +9°56'$

$n_2 = \cos\gamma_2 = 0.114;\ \gamma_2 = +83°27'$

and $\ell_3 = \cos\alpha_3 = 0.124;\ \alpha_3 = +82°52'$

$m_3 = \cos\beta_3 = 0.0633;\ \beta_3 = -86°35'$

$n_3 = \cos\gamma_3 = 0.988;\ \gamma_3 = +8°51'.$

Compatibility checks

In Table II all measured and computed parameters are summarized and in Figure 4 the stress distributions in planes 1-2, 2-3, and 3-1 are shown for each octant.

1. The first invariant, the sum of the principal stresses, $s_1 + s_2 + s_3 = 14 \times 10^{-2}$ lb/in.^{2}, is equal to the sum of the normal stresses, $\sigma_1 + \sigma_2 + \sigma_3 = 14.00 \times 10^{-2}$, indicating that the solution is accurate as far as the magnitudes of the principal stresses are concerned.

2. The curves connecting the ends of the corresponding stress vectors in planes 1-2, 2-3, and 3-1 are smooth and mirror-symmetric with respect to their main axes (Fig. 4).

Table II. Stresses and angular displacements
(all stresses in 10^{-2} lb/in.^{2}; + indicates compression).

	Measured	Computed	Measured	Computed	Measured	Computed
Plane	1-2		2-3		3-1	
Shear stresses	$\tau_{12} = +0.5$ $\tau_{64} = -2.5$		$\tau_{23} = +0.25$ $\tau_{45} = -1.5$		$\tau_{31} = -1$	
Normal stresses	$\sigma_1 = +9$	$\sigma_2 = +4$ $\sigma_6 = +7$ $\sigma_7 = +6$		$\sigma_3 = +1$ $\sigma_4 = +2.75$ $\sigma_8 = +2.25$		$\sigma_5 = +4$ $\sigma_9 = +6$
Maximum stresses						
Principal		$s_1 = +9.115$		$s_2 = +4.016$		$s_3 = +0.869$
Shear		$s^s_{12} = 2.549$		$s^s_{23} = 1.520$		$s^s_{31} = 4.123$
Angular displacement of principal stresses						
In space		$\alpha_1 = +8°30'$ $\alpha_2 = -85°57'$ $\alpha_3 = +82°52'$		$\beta_1 = +86°42'$ $\beta_2 = +9°50'$ $\beta_3 = -86°35'$		$\gamma_1 = -82°30'$ $\gamma_2 = +83°27'$ $\gamma_3 = +8°51'$

3. An extension of these curves over all four quadrants would show the expected four-leaved rose for the shear distribution and the required type of double cardioid for the normal stress distribution (Bernhard, 1961).

4. The directions of the zero shear-stress vectors coincide with the directions of the maximum and minimum normal-stress vectors, and the maximum shear-stress vectors bisect the angle between the adjacent maximum and minimum normal-stress vectors.

Comparison between shear stresses under static and dynamic loads

An arbitrary comparison is made between shear stresses under dynamic load (experimentally obtained) and under static load (theoretically computed).

For a static strip loading (biaxial system) the maximum shear stress at a point a is given by the equation:

$$s^s_{max} = \frac{p}{\pi} \sin \beta$$

where s^s_{max} = maximum shear stress

p = strip load

and β = angle of visibility (Figure 5).

Let $P_{total} = 500$ lb and $P_{strip} \simeq \frac{500}{1.5} \simeq 333$ lb

Strip area = $0.4 \times 1 = 0.4$ ft^2 = 57.6 in.^{2}

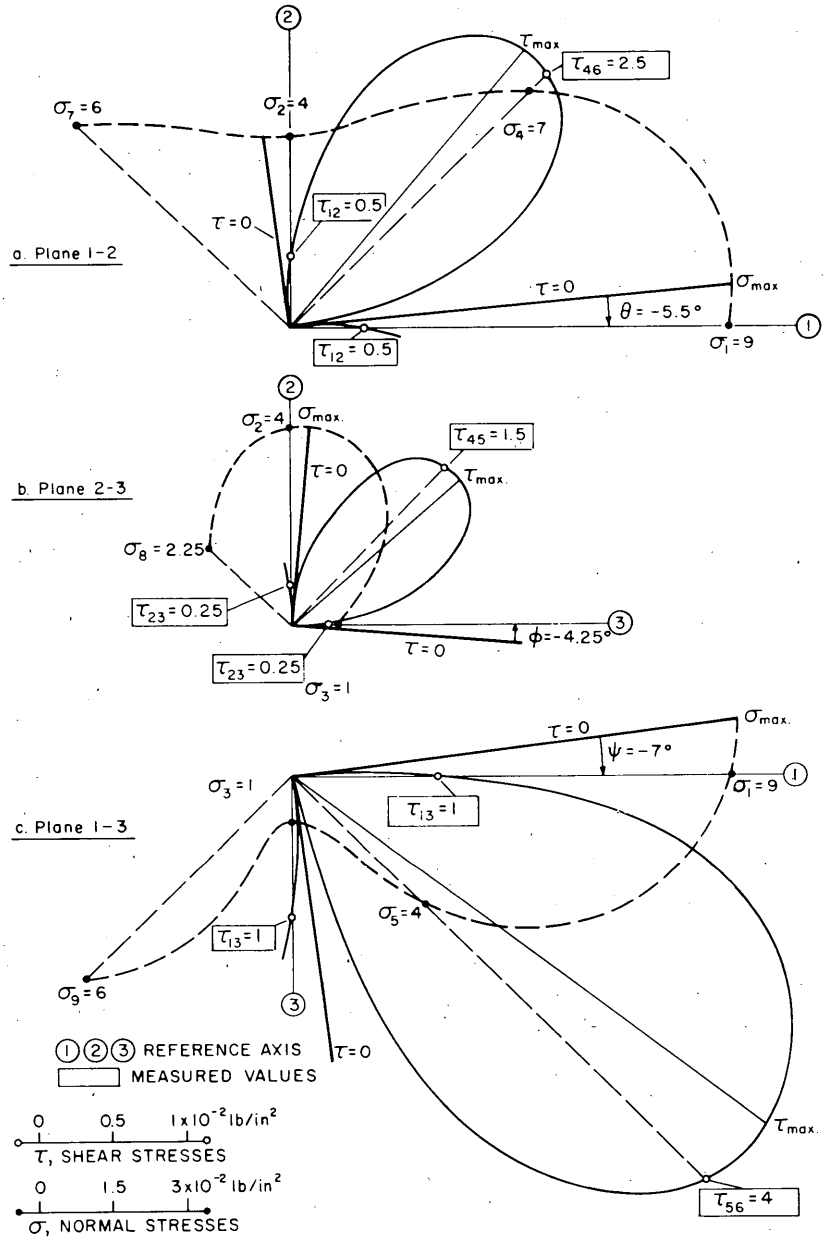

Figure 4. Stress distribution projected on planes 1-2, 2-3, 1-3.

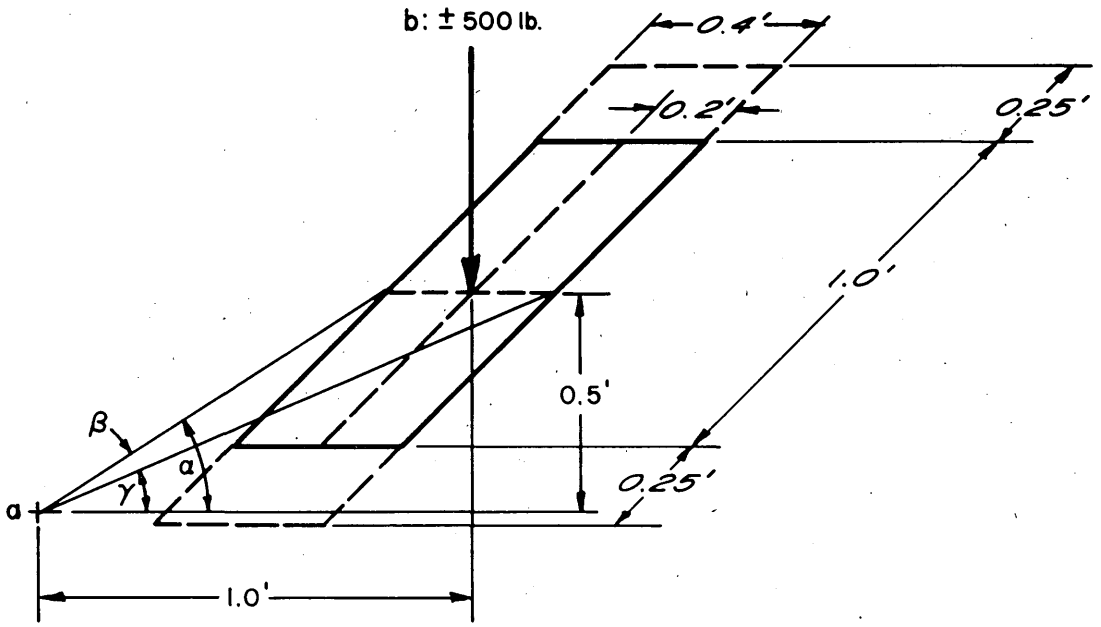

Figure 5. Maximum shear stress under a strip load.

then $\rho = \frac{333}{57.6} \cong 5.77$ lb/in.^{2}

From Figure 5 $\tan \alpha = \frac{0.5}{0.8} = 0.625$; $\alpha = 32°$

and $\tan \gamma = \frac{0.5}{1.2} = 0.416$; $\gamma = 22.6°$

and $\beta = \alpha - \gamma = 9.4°$; $\sin \beta = 0.163$

$s^s_{max} \cong \frac{5.77}{3.14}\ 0.163 \cong 0.3$ lb/in.^{2}

The corresponding maximum shear stress in the 1-2 plane due to a "dynamic" load of ± 500 lb, as determined experimentally, was approximately $\tau_{12}^{max} \cong 0.025$ lb/in.^{2} (Fig. 4a), which is much smaller than the computed static value of 0.3 lb/in.^{2} .

This seems to support indications of previous studies that under certain conditions the shear stresses in non-cohesive dry soils, when subjected to vibratory loads, may be substantially reduced in the vicinity of the exciter force.

Conclusions

From the measurements of five shear stresses and one normal stress the stress distribution of a triaxial system can be determined.

For non-cohesive, homogeneous, and isotropic soils, the elastic theory yields sufficiently accurate values.

The computed maximum stress at a point in dry sand under static strip loading is far greater than the maximum shear stress computed from observed data for the same dynamic load.

Further experimental and theoretical considerations are very desirable, particularly to study the effects of cohesion and of water content.

PART III. THREE-DIMENSIONAL NORMAL STRESS MEASUREMENTS

Introduction

Part II is based on the measurements of five shear and one normal stress. The shear stresses in the vicinity of the exciter source tend to approach very small values (fluidization) which might drop below the sensitivity threshold (noise level) of shear-measuring instruments.

These difficulties can be overcome by using six normal stress components, thus avoiding all shear components.

Furthermore in Part II all measurements were restricted to one particular point only. In Part III thirty-six points are investigated making the use of a computer imperative.

Experimental set-up

Instrumentation, measuring technique, and soil type were similar to those described in Part II.

The experimental set-up is shown in Figures 6 and 7. All measuring points are located within the "disturbed" zone; that is, in the immediate vicinity of the exciter force.

Thirty-six measuring points were selected under one quadrant of the contact plate (Fig. 6), 12 each at 8, 12, and 16 inches below the contact plate which is 20 inches square.

At each location three pressure cells in an orthogonal arrangement (Fig. 7a), and three pressure cells in a non-orthogonal arrangement (Fig. 7b) were buried consecutively*. Thus a total of 216 stress components each averaged from the individual measurements have been included in the evaluation.

The sinusoidal force vector was restricted to ±1000 lb vertical force and frequency of 25 cps to reduce the computational effort.

Results

All measured parameters are summarized in Table III. Negative values indicate a decrease in pressure, representing a loosening effect instead of a densifying effect.

The principal stresses and their direction cosines were evaluated with an IBM 1620 computer using the six averaged normal stresses "measured" at each of the thirty-six points. A total of 432 unknown parameters had to be determined.

A short description of the method used to evaluate the principal stresses and their direction cosines from the "measured" normal stress components is given in Appendix B.

*The output of only one cluster of these pressure cells was recorded at a time to avoid distortion from adjacent measuring points.

For simplicity the computation derived from the experimental results is based on the rather controversial assumption that the soil can be considered as an elastic, homogeneous, isotropic, half-space continuum.

In Table IV, the principal stresses with their direction cosines are summarized.

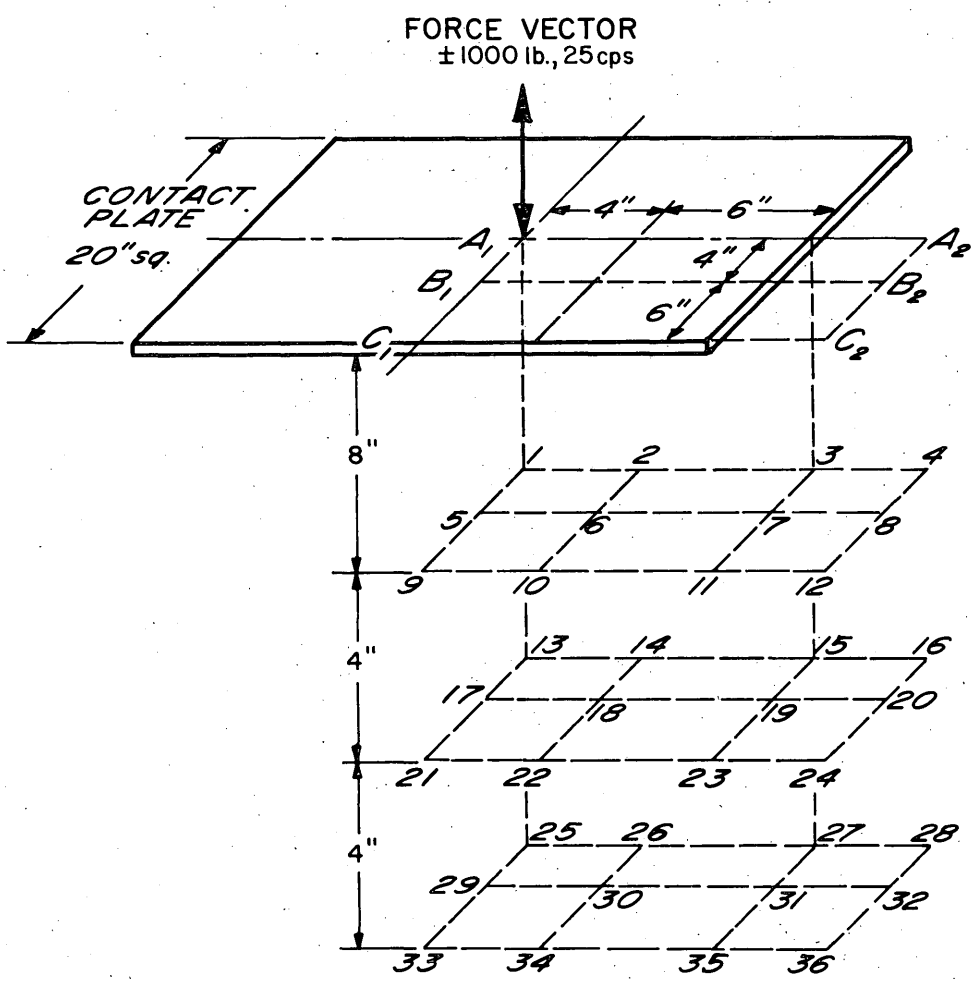

Figure 6. Experimental set-up.

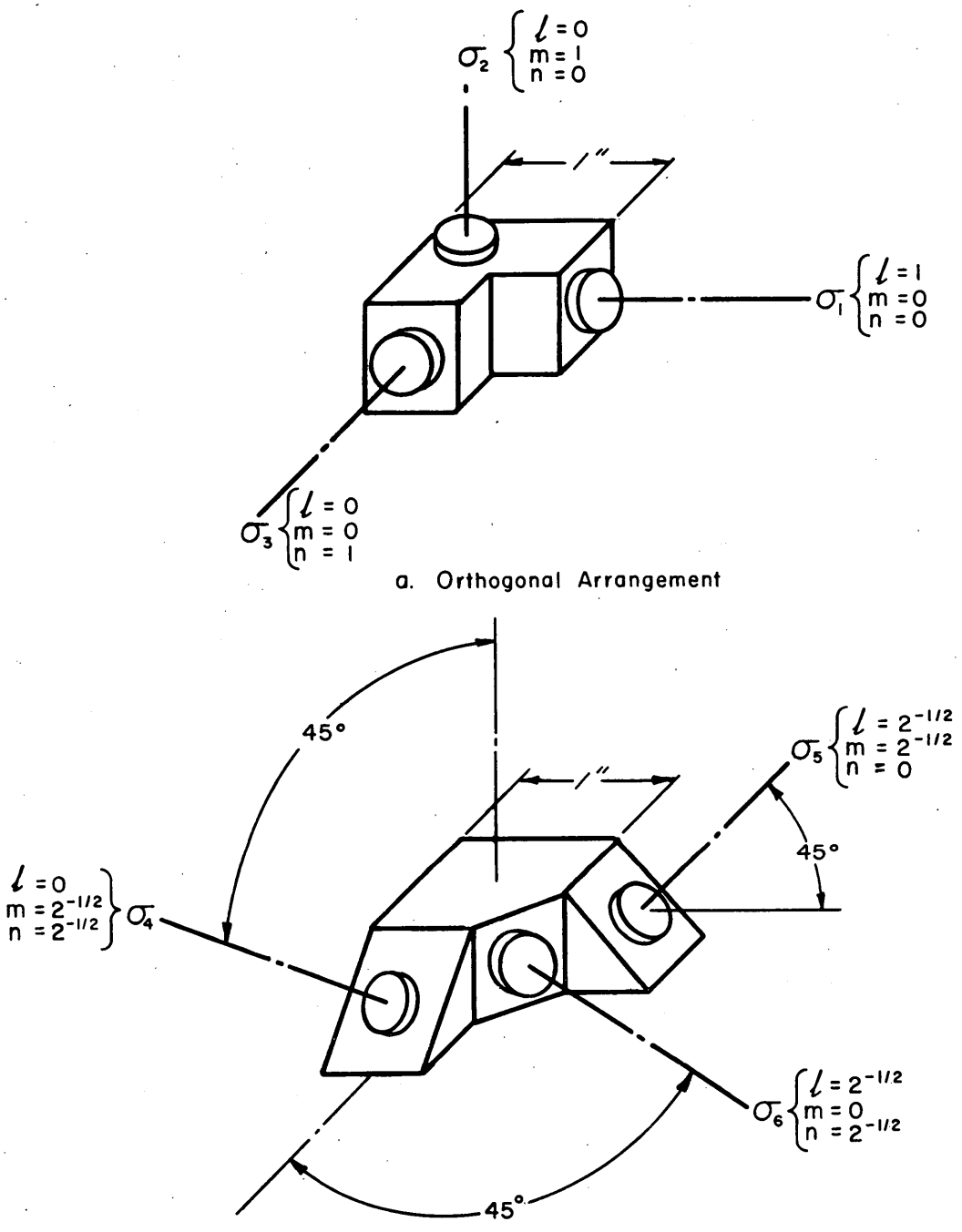

Figure 7. Orientation of differential pressure cells at each point.

Table III. "Measured" normal stress components, psi.

Locations 1-12 (8-in. deep)

	1	2	3	4	5	6	7	8	9	10	11	12
σ_1	0.18	0.20	0	0	0.10	0	0	0	-0.06	-0.04	-0.04	0
σ_2	4.00	1.24	0.26	0	3.44	0.68	0.20	0	0.30	0.28	0.24	0
σ_3	0.30	0	0.08	0.06	0.36	0.04	0	0	-0.28	-0.24	-0.22	0
σ_4	1.86	0.12	0.30	0	2.20	1.36	0.06	0	0.24	0.32	0.48	0
σ_5	0.14	0.30	0.04	0	0.04	0.02	0.02	0.02	0.48	0.44	0.66	0.02
σ_6	2.80	2.40	2.16	0.20	0.44	0.30	0.56	0.44	0.14	0.18	0.52	0.04

Locations 13-24 (12-in. deep)

	13	14	15	16	17	18	19	20	21	22	23	24
σ_1	-0.06	-0.06	-0.06	0	-0.12	-0.10	0.16	-0.08	0.04	-0.12	-0.08	-0.04
σ_2	1.38	1.38	1.00	0.60	0.38	0.44	0.38	0.12	0.44	0.42	0.44	0.40
σ_3	-0.24	-0.24	-0.12	0.24	0.10	0.10	-0.32	0.06	-0.10	-0.30	-0.28	-0.20
σ_4	1.24	0.80	0.24	0.20	1.80	2.00	0.36	0.28	0.24	0.32	0.32	0.30
σ_5	0.06	0.04	0.02	0.02	0.02	0.34	0.54	0.10	0.54	0.50	0.50	0.40
σ_6	1.36	1.42	1.86	0.36	0.32	1.74	0.50	0.12	0.18	0.18	0.24	0.18

Locations 25-36 (16-in. deep)

	25	26	27	28	29	30	31	32	33	34	35	36
σ_1	0	-0.10	-0.10	-0.10	0	0	0	0	0	0	0	0
σ_2	1.12	1.20	0.90	0.90	0.60	0.50	0.40	0.16	0.42	0.40	0.26	0.20
σ_3	-0.40	-0.24	-0.24	-0.20	0	0	0	0.02	0.02	0.02	0.02	0.02
σ_4	0.32	0.62	0.56	0	0.84	0.64	0.50	0.18	0.92	0.80	0.60	0.40
σ_5	0	0	0	0	0.16	0.24	0.34	0.18	0.26	0.30	0.40	0.20
σ_6	0.96	2.00	1.84	0.20	0.04	0.04	0.04	0.02	0.04	0.40	0.42	0.02

Table IV. Principal stresses and direction cosines.

8-in. depth

Location	Principal stresses, psi			Direction cosines		
	S_1	S_2	S_3	ℓ	m	n
	0.04	-	-	0.967	-0.159	0.197
(1)	-	4.15	-	0.177	0.981	-0.078
	-	-	0.29	-0.181	0.111	0.977
	-1.21	-	-	0.735	-0.576	-0.358
(2)	-	2.51	-	0.578	0.808	-0.115
	-	-	0.14	0.356	-0.122	0.927
	-1.91	-	-	0.728	-0.684	0.045
(3)	-	2.17	-	0.683	0.729	0.045
	-	-	0.08	-0.064	-0.002	0.998
*(4)	-	-	-	-	-	-
	-0.37	-	-	0.941	0.319	0.113
(5)	-	3.94	-	-0.330	0.939	0.096
	-	-	0.34	-0.075	-0.128	0.989
	0.00	-	-	0.999	-0.002	0.041
(6)	-	1.41	-	-0.023	0.808	0.589
	-	-	-0.69	-0.034	0.590	0.807
(7)	-0.38	-	-	0.773	-0.626	-0.108
	-	0.57	-	0.626	0.779	-0.033
	-	-	0.00	0.104	-0.042	0.994
(8)	-	-	-	-	-	-
	0.59	-	-	0.614	0.518	0.596
(9)	-	0.22	-	-0.482	0.844	-0.237
	-	-	-0.85	-0.626	-0.142	0.767
(10)	0.63	-	-	0.557	0.596	0.579
	-	0.14	-	-0.570	0.781	-0.256
	-	-	-0.77	-0.604	-0.188	0.755
	1.11	-	-	0.592	0.583	0.556
(11)	-	-0.20	-	-0.488	0.809	-0.329
	-	-	-0.93	-0.641	-0.076	0.764
*(12)	-	-	-	-	-	-

* Values approach zero since the point is beyond the contact plate.

Table IV. (Cont'd).

12-in. depth

Location	Principal stresses, psi			Direction cosines		
	S_1	S_2	S_3	ℓ	m	n
(13)	-0.32	-	-	0.911	-0.244	-0.331
	-	1.89	-	0.350	0.883	0.312
	-	-	-0.49	0.216	-0.400	0.891
(14)	-0.43	-	-	0.831	-0.288	-0.476
	-	1.75	-	0.396	0.907	0.143
	-	-	-0.24	0.391	-0.307	0.868
(15)	-1.06	-	-	0.801	-0.560	-0.212
	-	1.96	-	0.564	0.824	-0.049
	-	-	-0.08	0.203	-0.080	0.976
(16)	-0.07	-	-	0.867	-0.225	-0.444
	-	0.70	-	0.017	0.905	-0.425
	-	-	0.20	0.497	0.361	0.789
(17)	-0.12	-	-	0.993	-0.002	-0.120
	-	1.82	-	0.083	0.737	0.670
	-	-	-1.34	0.088	-0.675	0.732
(18)	-1.94	-	-	0.502	-0.700	0.509
	-	2.73	-	0.459	0.714	0.529
	-	-	-0.35	-0.732	-0.032	0.680
(19)	0.98	-	-	0.569	0.649	0.506
	-	-0.05	-	-0.473	0.761	0.444
	-	-	-1.02	-0.673	0.013	0.739
(20)	-0.14	-	-	0.857	0.045	-0.513
	-	0.33	-	0.335	0.707	0.623
	-	-	-0.09	0.390	-0.706	0.591
(21)	0.59	-	-	0.722	0.210	0.659
	-	0.44	-	-0.196	0.975	-0.096
	-	-	-0.64	-0.663	-0.060	0.746
(22)	0.67	-	-	0.525	0.643	0.557
	-	0.28	-	-0.558	0.755	-0.345
	-	-	-0.95	-0.643	-0.129	0.755
(23)	0.68	-	-	0.529	0.657	0.537
	-	0.28	-	-0.560	0.746	-0.361
	-	-	-0.88	-0.638	-0.109	0.763
(24)	0.54	-	-	0.461	0.722	0.517
	-	0.28	-	-0.624	0.677	-0.390
	-	-	-0.67	-0.631	-0.143	0.762

Table IV. (Cont'd).

16-in. depth

Location	Principal stresses, psi			Direction cosines		
	S_1	S_2	S_3	ℓ	m	n
	-0.01	-	-	0.836	-0.258	0.485
(25)	-	1.25	-	0.303	0.953	-0.015
	-	-	-0.52	-0.458	0.160	0.874
	-1.04	-	-	0.839	-0.537	-0.084
(26)	-	2.16	-	0.543	0.835	0.087
	-	-	-0.25	0.023	-0.119	0.993
	-1.12	-	-	0.815	-0.579	-0.006
(27)	-	1.96	-	0.575	0.808	0.129
	-	-	-0.28	-0.070	-0.108	0.992
	0.01	-	-	0.833	-0.030	0.553
(28)	-	1.02	-	-0.136	0.957	0.257
	-	-	-0.04	-0.537	-0.289	0.792
	0.13	-	-	0.849	-0.123	0.515
(29)	-	0.94	-	-0.160	0.868	0.471
	-	-	-0.48	-0.504	-0.482	0.717
	0.22	-	-	0.805	-0.182	0.565
(30)	-	0.72	-	-0.111	0.889	0.444
	-	-	-0.44	-0.583	-0.420	0.695
	0.30	-	-	0.776	-0.348	0.527
(31)	-	0.56	-	0.053	0.867	0.495
	-	-	-0.46	-0.629	-0.356	0.691
(32)	-0.19	-	-	0.684	0.288	-0.671
	-	0.21	-	0.268	0.755	0.598
	-	-	0.16	0.679	-0.589	0.439
	0.14	-	-	0.908	-0.266	0.323
(33)	-	0.96	-	0.017	0.795	0.606
	-	-	-0.66	-0.418	-0.545	0.727
	-0.08	-	-	0.891	-0.449	0.063
(34)	-	0.95	-	0.334	0.745	0.578
	-	-	-0.45	-0.306	-0.494	0.814
	-0.17	-	-	0.707	-0.680	0.194
(35)	-	0.87	-	0.479	0.662	0.577
	-	-	-0.42	-0.521	-0.315	0.793
	0.12	-	-	0.835	-0.427	0.348
(36)	-	0.42	-	0.135	0.771	0.623
	-	-	-0.32	-0.534	-0.473	0.701

Computed principal stress components. In Figure 9 the trends shown in Table III are still more obvious.

In addition the tendency of larger stresses under the centerline A_1 - A_2, particularly at the 8" and 16" level, is clearly discernible, with the maximum at point 1 directly under the exciter force.

Furthermore the maximum principal stresses are not confined to the s_1 values computed from the cubic equation for the three principal stresses s_1, s_2, and s_3. At the 16" level, for example, the s_2 values predominate throughout (Table IV).

The horizontal stress components under the center, A_1, of the contact plate do not approach zero, showing the difficulty in placing as well as keeping the pressure cells exactly in their original positions during vibration. The discrepancy may be due to some heterogeneity of the soil.

Comparison with static loads. Points 11, 23, and 35 under corner C_2 of the contact plate were used to compare the effects of dynamic and static loads. The vertical stress component (σ_2) due to a static load of 1000 lb was computed using Steinbrenner's method (1934), keeping in mind that the method may not be valid in the "disturbed zone." The results of this comparison (Table V) indicate that the maximum dynamic values are larger than the static values and follow a different pattern.

In addition, Table V compares the computed static values (σ_2) and the computed maximum principal stresses (s_{max}). A further increase in stress due to dynamic loading is evident and reflects the value of the 45° measurements.

Table V. Comparison of stresses due to static and dynamic loads, psi.

		Static	Dynamic	
Location	Depth	Computed σ_2	Measured σ_{max}	Computed S_{max}
11	8"	0.498	0.66	1.11
23	12"	0.476	0.50	0.68
35	16"	0.414	0.60	0.87

Analysis

"Measured" normal stress components. The significant values (Table III) show a general decrease at greater depth and distance from the exciter source. The tendency of the direction of the maximum stress vectors to point from the exciter source becomes obvious (Fig. 9).

The almost negligible effect beyond the contact plate at the 8" level (points 4, 8, and 12) shows that the points are beyond the range of instrument sensitivity.

Polar diagrams (Fig. 8) indicate that the six "measured" normal stress components do not follow a pattern that would have been expected under static loads, that is, a steady decrease in magnitude with increase in depth and distance.

In particular the stresses under C_1, considering points 9 and 21, show a pressure decrease or loosening rather than a densification effect in the vicinity of the outer edge of the contact plate.

A similar phenomenon appears under C_2 (points 11 and 35). However, the decrease in compaction effect is confined to the 2-3 plane only.

Furthermore, with the exception of the stresses under C_1 in the 1-2 plane, the maximum stresses are predominantly the 45° components, in particular for the deepest points 33 and 35 in the 2-3 plane. Thus the importance of measuring the 45° components cannot be overemphasized.

Conclusions

The following tentative conclusions may be drawn:

1. In non-cohesive soils triaxial stress fields due to vibratory loads can be determined by recording six independent stress components.

2. The measuring technique that was used seems adequate.

3. Dynamic loads and static loads have different patterns.

4. Under dynamic loads the vertical stress component ceases to be of critical significance, particularly in the disturbed zone.

5. Further investigations at greater depths and with special regard to the horizontal and 45° components, and with other types of soils, different moisture contents, and forces are necessary.

6. Substantially more parameters, including viscoelastic characteristics, have to be determined before an attempt can be made to develop a mathematical model covering the effect of dynamic loads.

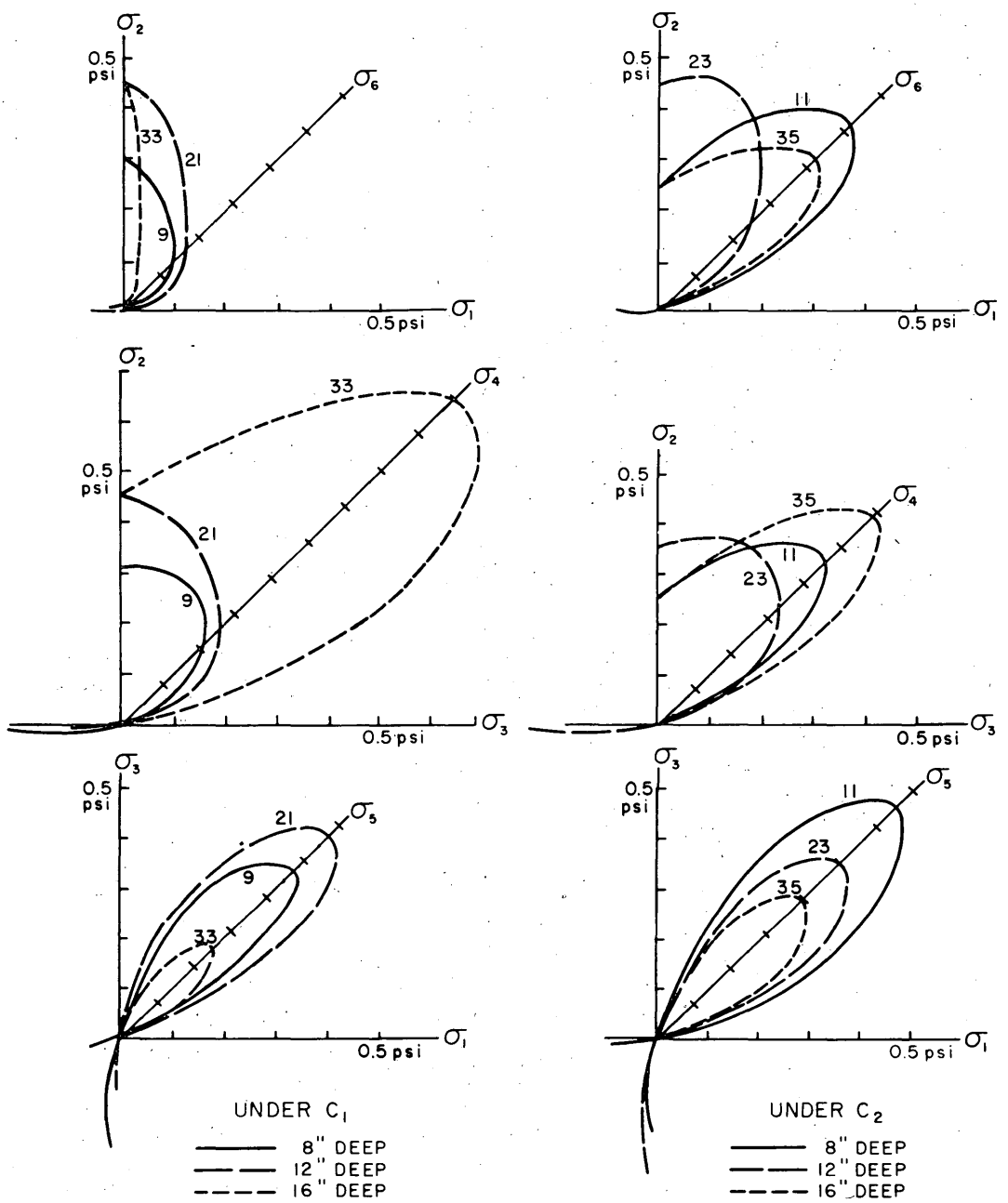

Figure 8. Measured normal stress components in polar coordinates under C_1 and C_2 of contact plate.

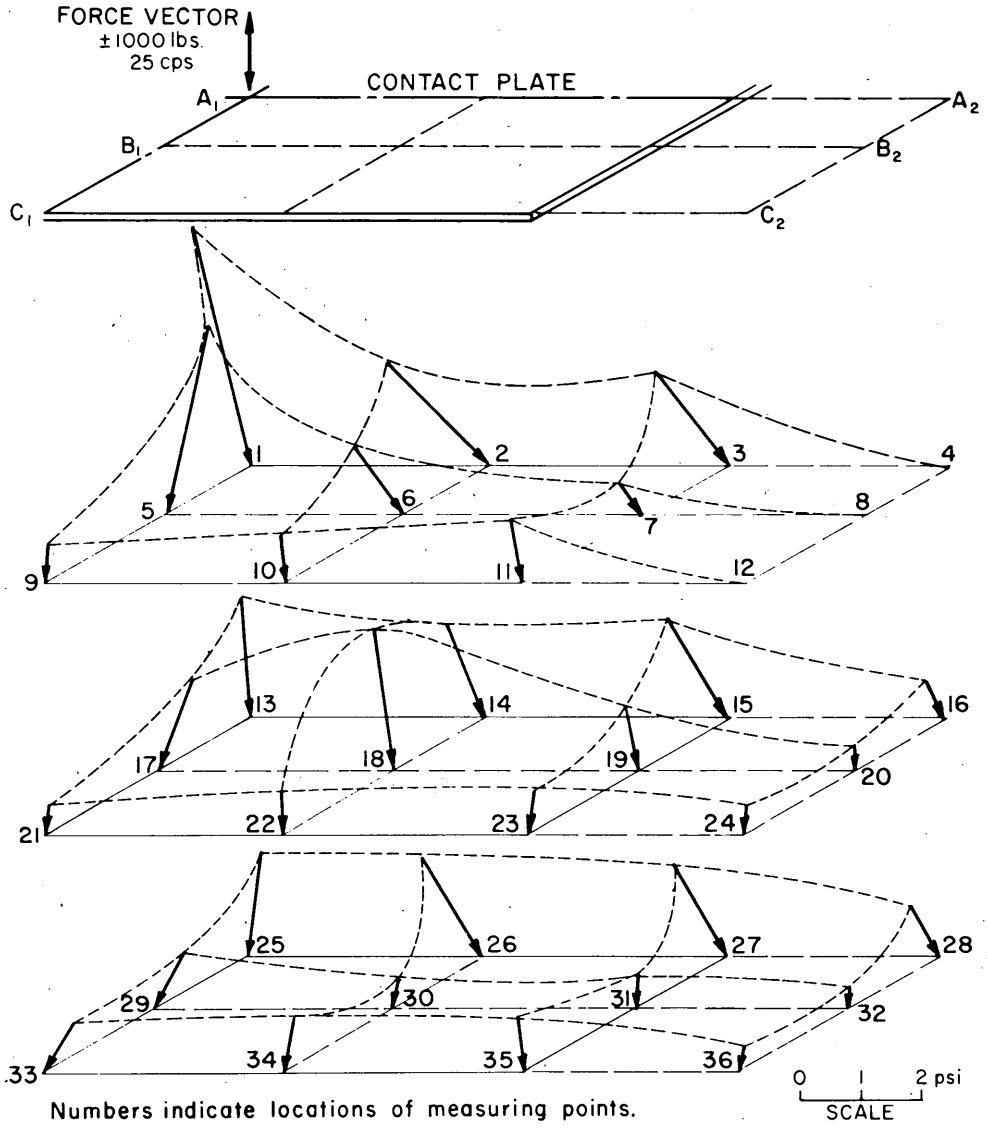

Figure 9. Computed maximum principal stresses.

PART IV. SOIL WAVE PROPAGATION IN STRATIFIED SOIL

Introduction

Snow and ice in cold regions are usually stratified. Among the methods used to determine the depth of soil strata, some are based on distance-time graphs obtained from the velocity of waves propagated through these strata. The waves may be excited by sinusoidal, or by impact, forces.

The following analyses are presented to demonstrate that sinusoidal force excitation and impact excitation yield time-distance graphs which can be used to determine reflection and refraction techniques in stratified soils.

The three analyses are based upon a summarization of the referenced technical literature (see Selected Bibliography) and upon the further development of some of the derivations from the references.

For all investigations, homogeneous soils with horizontal strata interfaces are assumed.

Distance-time graphs

Purpose. To present an analytical proof that under certain conditions of sinusoidal force excitation – independent of the assumed ray path — the distance-time graph of wave propagation in a two-strata formation will yield two almost straight lines. The lines have a breaking point at a critical distance from the disturbing source (Bernhard, 1936; 1958). The slope of the lines before this critical point represents the phase velocity in the upper stratum; the slope of the lines beyond represents the apparent phase velocity in the lower stratum.

Procedure. Let the soil be considered as an isotropic, homogeneous, elastic, half-space continuum.

From energy losses due to expansion and absorption, the decrease in displacement amplitudes with increase in distance from the exciter source can be determined.

Assuming a stratified soil comprising two layers, the phase angle between the (direct) surface wave and the (indirect) refracted wave is discussed.

Finally, the phase velocities and the distance-time graphs are analyzed.

Notation – Part IV

d = distance
h = depth of a stratum
i = angle of waveray (pencil)
n = frequency
r = order number
s = distance
t = time
v = velocity
x = vertical displacement amplitude
E_0 = total energy of sphere of unit radius
E = potential energy
E^{kin} = kinetic energy
ω = angular velocity. circular frequency.
λ = wave length
μ = absorption coefficient
τ = displacement amplitude ratio
θ = phase constant
ϕ = phase angle

Energy loss due to spherical expansion.

Let E_o = total energy of sphere with radius r = 1

dA = elementary area

$4\pi r^2$ = area of sphere, where r = radius of sphere

$d_a < d_b$ = distances from source to point a and to point b

$x_a > x_b$ = vertical displacement amplitudes at points a and b

dm = elementary mass

$x = x^{max} \sin(\omega t - \phi)$.

Potential energy at points a and b:

$$E_a = \frac{E_o\, dA}{4\pi d_a^2}, \quad E_b = \frac{E_o\, dA}{4\pi d_b^2} \quad \text{or} \quad \frac{E_a}{E_b} = \frac{d_b^2}{d_a^2}.$$

Kinetic energy at points a and b:

$$\max E_a^{kin} = \frac{\omega x_a^2}{2}\, dm, \quad \max E_b^{kin} = \frac{\omega x_b^2}{2}\, dm$$

or

$$\max \frac{E_a^{kin}}{E_b^{kin}} = \frac{x_a^2}{x_b^2}.$$

Finally, $\frac{d_b^2}{d_a^2} = \frac{x_a^2}{x_b^2}$ and $x_2 = x_a \frac{d_a}{d_b}$. (1)

Energy loss due to absorption. Energy losses due to absorption require an additional decay factor:

$$e^{-\mu(d_a - d_b)} \tag{2}$$

where μ = absorption coefficient.

A combination of eq 1 and 2 yields (Heinrich, 1930; Biot, 1956):

$$x_b = x_a \frac{d_a}{d_b} e^{-\mu(d_b - d_a)}. \tag{3}$$

Ray path. Let detectors A and B on the soil surface have the distances d and d' from the exciter (Fig. 10). Detector A will pick up the wave along the surface (direct path) with the vertical displacement amplitude x_1 and the phase θ_1, and the wave refracted from the lower stratum (indirect path) with the

amplitude x_2 and the phase θ_2. The corresponding values for detector B are: x'_1, θ'_1 and x'_2, and θ'_2. The velocity is v_1 in the upper stratum and v_2 in the lower stratum.

The shape of the indirect ray pencil is irrelevant in the following considerations.

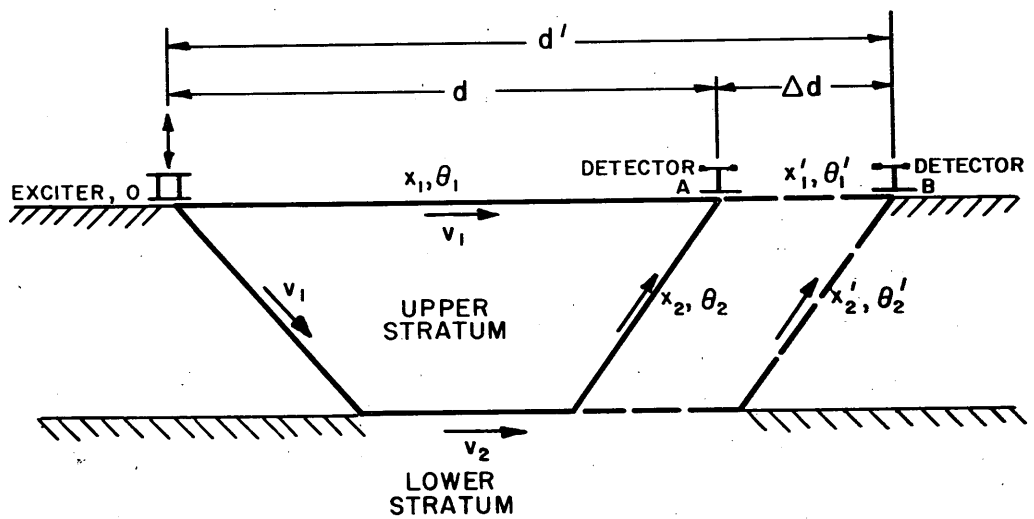

Figure 10. Ray paths through two strata-sinusoidal force excitation: refraction.

Phase constant. The phase constant between the two detectors Δd apart must have the form:

$$\omega\theta' - \omega\theta = F(x'_1\ \theta'_1\ x'_2\ \theta'_2\ x_1\ \theta_1\ x_2\ \theta_2)$$

$$\text{or } \tan(\omega\theta' - \omega\theta) \text{ where } \begin{cases} \tan\omega\theta' = \dfrac{x'_1\sin\omega\theta'_1 + x'_2\sin\omega\theta'_2}{x'_1\cos\omega\theta'_1 + x'_2\cos\omega\theta'_2} = \dfrac{A}{B} \\ \tan\omega\theta = \dfrac{x_1\sin\omega\theta_1 + x_2\sin\omega\theta_2}{x_1\cos\omega\theta_1 + x_2\cos\omega\theta_2} = \dfrac{C}{D} \end{cases} \tag{4}$$

$$\tan(\omega\theta' - \omega\theta) = \frac{\tan\omega\theta' - \tan\omega\theta}{1+\tan\omega\theta'\tan\omega\theta} = \frac{A/B - C/D}{1+A/B\,C/D} = \frac{AD-BC}{BD+AC} =$$

$$= \frac{x'_1x_1\sin\omega(\theta'_1-\theta)+x'_1x_2\sin\omega(\theta'_1-\theta_2)+x'_2x_1\sin\omega(\theta'_2-\theta_1)=x'_2x_2\sin\omega(\theta'_2-\theta_2)}{x'_1x_1\cos\omega(\theta'_1-\theta)+x'_1x_2\cos\omega(\theta'_1-\theta_2)+x'_2x_1\cos\omega(\theta'_2-\theta_1)+x'_2x_2\cos\omega(\theta'_2-\theta_2)}. \tag{5}$$

Divide by $x_1x'_1$ and substitute for $\frac{x_2}{x_1} = \tau$ and for $\frac{x'_2}{x'_1} = \tau'$, then:

$$\tan\omega(\theta'-\theta) = \frac{\sin\omega(\theta'_1-\theta_1)+\tau'\sin\omega(\theta'_2-\theta_1)+\tau\sin\omega(\theta'_1-\theta_2)+\tau\tau'\sin\omega(\theta'_2-\theta_2)}{\cos\omega(\theta'_1-\theta_1)+\tau'\cos\omega(\theta'_2-\theta_1)+\tau\cos\omega(\theta'_1-\theta_2)+\tau\tau'\cos\omega(\theta'_2-\theta_2)}. \tag{6}$$

Phase velocity. For τ and $\tau' \ll 1$, that is, the amplitudes of the direct path are larger than that of the indirect path:

$\tan\omega(\theta'-\theta) = \tan\omega(\theta_1'-\theta_1)$, representing the first terms of eq 6, and since $\theta_1 = \frac{d}{v_1}$ for the upper stratum

$$\theta'-\theta = \frac{d'-d}{v_1} \quad \text{or} \quad v_1 \sim \frac{\Delta d}{\theta_1-\theta} .$$

Hence, the wave velocity of the resultant wave is equal to v_1 of the upper stratum.

For τ and $\tau' \gg 1$, that is, the amplitudes of the direct path are smaller than that of the indirect path:

$\tan\omega(\theta'-\theta) = \tan\omega(\theta_2'-\theta_2)$, representing the last terms of eq 6 and, since $\theta_2 = \frac{d}{v_2}$ for the lower stratum,

$$\theta'-\theta = \frac{d'-d}{v_2} \quad \text{or} \quad v_2 \sim \frac{\Delta d}{\theta'-\theta} .$$

Hence, the velocity of the resultant wave is equal to v_2 of the lower stratum.

For τ and $\tau \sim 1$:

Upper stratum: Let $x_b = x_1$, $x_a = x_{10}$, and $d_a = 1$, $d_b = d'$, $\mu = \mu_1$.

Eq 3 changes into

$$x_1 = x_{10} \frac{1}{d'} e^{-\mu_1(d'-1)} . \tag{7}$$

Lower stratum: Let $x_b = x_2$, $x_a = x_{20}$, and make $d_a = 1$, $d_b = d_b = d'$, $\mu = \mu_2 < \mu_1$. Eq 3 changes into:

$$x_2 = x_{20} \frac{1}{d'} e^{-\mu_2(d'-1)} \tag{8}$$

or

$$\frac{x_2}{x_1} = \frac{x_{20}}{x_{10}} e^{+(\mu_1-\mu_2)(d'-1)} .$$

Since $x_2 = x_1$, that is, both amplitudes are equal at distance d', substituting $A^{-1} = \frac{x_{20}}{x_{10}}$ gives:

$$1 = \frac{e^{(\mu_1-\mu_2)(d'-1)}}{A} \quad \text{or} \quad \ln 1 = (\mu_1-\mu_2)d'-(\mu_1-\mu_2)-\ln A$$

$$0 = d' - 1 - \frac{\ln A}{\mu_1-\mu_2} .$$

and

$$d' = 1 + \frac{\ln A}{\mu_1 - \mu_2} \quad . \tag{9}$$

Distance versus time. For

$$\tau = \frac{x_2}{x_1} = \frac{x_{20}}{x_{10}} = 1 \text{ or } \ln A = 0$$

Eq 9 yields:

$$d' = 1 + \frac{0}{\mu_1 - \mu_2} = 1$$

and, as derived previously, whenever

$$\left.\begin{aligned} \tau &= \frac{x_2}{x_1} < 1 \\ \text{and} \quad \tau' &= \frac{x'_2}{x'_1} < 1 \end{aligned}\right\} \; d<d' \text{ and } v_1 \text{ govern}$$

and when

$$\left.\begin{aligned} \tau &= \frac{x_2}{x_1} > 1 \\ \text{and} \quad \tau' &= \frac{x'_2}{x'_1} > 1 \end{aligned}\right\} \; d>d' \text{ and } v_2 \text{ govern.}$$

Results

Summarizing the results it can be stated that the distance-time graph forms a broken line, provided that the absorption coefficient of the upper stratum is larger than the absorption coefficient of the lower stratum and that the displacement amplitudes at the origin are larger for the stratum with the larger absorption coefficient.

Sinusoidal force excitation

Purpose. To show that sinusoidal force excitation on stratified soil yields time-distance graphs which can be used to determine reflection and refraction effects.

The following derivations (Kohler, 1936; Kohler and Ramspeck, 1936; Ramspeck and Schulze, 1938; Bernhard, 1936b; Converse et al., 1952, 1954, 1955) are based on the relationship:

1. Time versus distance
2. Displacement versus frequency
3. Displacement versus distance

The first correlation yields the apparent phase velocity, the second the order number, and the third the interference maxima or minima of the resultant vertical component of the trajectory.

Reflection and refraction effects will be discussed separately.

Reflection.

Interference maxima: The assumption is made that of two interfering waves one follows a straight line path O-A along the surface of the upper stratum and the other a broken path O-B-A, reflected at B from the lower stratum (Fig. 11). Let the wave-propagation velocity in the upper stratum be v_1. The velocity in the lower stratum does not enter into this case. The distance between the exciter O and the detector A = d; the depth of the upper stratum = h; and the distance between the exciter O, or the detector A, and the reflection point B is $\overline{OB} = \overline{AB} = \frac{s}{2}$.

Then

$$s = \sqrt{d^2 + 4h^2}$$

the traveling times: $t_1 = \frac{d}{v_1}$ and $t_2 = \frac{s}{v_1} = \frac{\sqrt{d^2 + 4h^2}}{v_1}$,

and the time difference: $\Delta t = t_2 - t_1 = \frac{1}{v_1} = \left[\sqrt{d^2 + 4h^2} - d\right]$ (10)

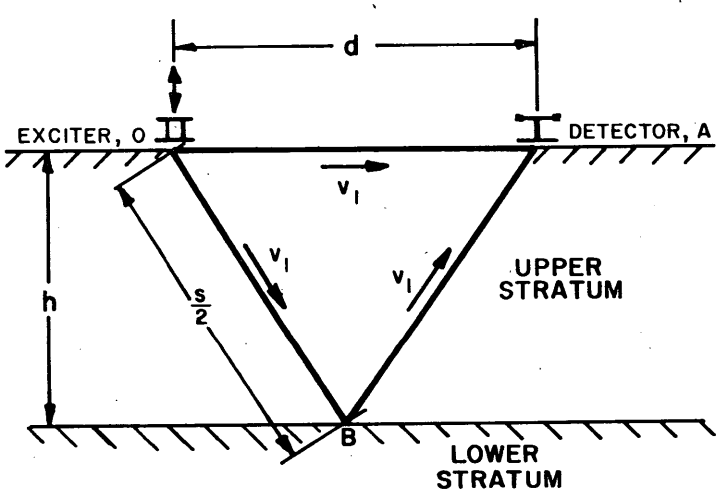

Figure 11. Ray paths through two strata-sinusoidal force excitation: reflection.

Distance between two adjacent maxima: An interference maximum or minimum of the resultant displacement amplitudes at A is formed whenever

$$\cos(2\pi n \Delta t) = \pm 1,$$

where n = wave frequency (cps).

Only maxima are discussed from here on.

Hence $\cos 2\pi n \left[\frac{1}{v_1}\left(\sqrt{d^2 + 4h^2} - d\right)\right] = +1.$

Let r represent the order number (0, 1, 2, 3----), then

$$2\pi n \left[\frac{1}{v_1} \left(\sqrt{d^2 + 4h^2} - d\right)\right] = 2\pi r$$

or

$$\frac{1}{v_1} \left(\sqrt{d^2 + 4h^2} - d\right) = \frac{r}{n}. \tag{11}$$

Substitute $v_1 = n\lambda$ where λ = wave length (feet)

$$\frac{1}{n\lambda} \left(\sqrt{d^2 + 4h^2} - d\right) = \frac{r}{n}$$

and

$$\sqrt{d^2 + 4h^2} = r\lambda + d$$

$$4h^2 = r^2\lambda^2 + 2rd\lambda \tag{12}$$

$$2rd\lambda = 4h^2 - r^2\lambda^2,$$

Finally:

$$d = \frac{4h^2 - r^2\lambda^2}{2r\lambda}. \tag{13}$$

The smaller the order number r, the greater the distance d between exciter O and detector A. Hence for the largest distance d at which an interference maximum can still occur, the order number r must be equal to one.

Let the distance of two adjacent displacement maxima for constant n be:

$$\Delta d = d_2 - d_1.$$

Substitute $q = 2r$ or $r = \frac{q}{2}$ into eq 12, then

$$4h^2 = \frac{q_2^2}{4}\lambda^2 + q_2 d_2 \lambda$$

$$4h^2 = \frac{q_1^2}{4}\lambda^2 + q_1 d_1 \lambda$$

or

$$\frac{\lambda^2}{4}(q_2^2 - q_1^2) + \lambda(q_2 d_2 - q_1 d_1) = 0 \tag{14}$$

where $q_2 < q_1$ since $d_2 > d_1$

hence $q_2 = 2r_1$

and, for $r_1^{min} = 1$ or $q_2 = 2$

$q_1 = 2r_2$

and, for $r_2 = 2$ or $q_1 = 4$, $q_1 = q_2 + 2$.

Replacing q_1 by $q_2 + 2$ in eq 14 yields:

$$\lambda [q_2^2 - (q_2 + 2)^2] + 4 \{q_2 d_2 - [(q_2 + 2) d_1]\} = 0$$

$$(-4q_2 - 4)\lambda + 4 [q_2 (d_2 - d_1) - 2d_1] = 0$$

$$-(q_2 + 1) \lambda + q_2 \Delta d - 2d_1 = 0$$

$$\Delta d = \frac{2d_1 + (q_2 + 1)\lambda}{q_2}$$

and finally

$$\Delta d = \frac{2d + (2r+1) \lambda}{2r} \quad . \tag{15}$$

In the case of reflection, the distance Δd between two adjacent interference maxima increases with the distance d between the exciter at O and the detector at A. This is not the case for refraction, as discussed later.

Maximum distance of interference maxima from disturbing force:

Since $r^{min} = 1$, for d^{max}, from eq 13:

$$d^{max} = \frac{4h^2 - \lambda^2}{2\lambda} \quad .$$

Whenever interference maxima are observed at a distance between the exciter at O and the detector at B larger than d^{max}, reflection effects cannot take place and refraction phenomena must be considered.

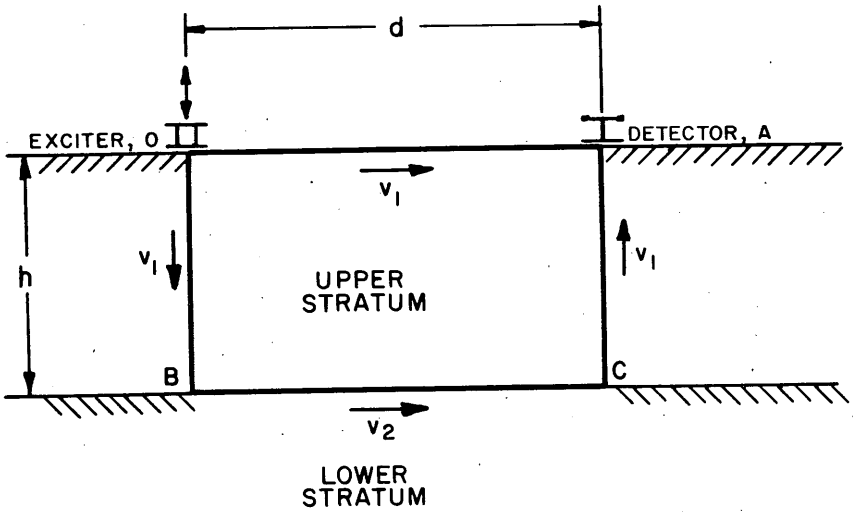

Figure 12. Ray path – two strata – sinusoidal force excitation: refraction.

Refraction

Two cases, a two-strata and a three-strata formation, will be discussed.

Case I. A low-velocity stratum on a high-velocity stratum: Let Figure 12 represent a ray path diagram. For simplicity's sake the indirect path O-B-C-A is assumed to be U-shaped; that is, OB in Figure 15 is equal to h, or i_1 in Figure 17a approaches zero ($v_1 \ll v_2$). It must be clearly understood that this shape does not represent the correct path, the exact form of which is unknown. In many cases, however, no significant errors are caused by this arbitrary assumption.

The traveling times for the direct and indirect path are:

$$t_1 = \frac{d}{v_1} \text{ and } t_2 = \frac{2h}{v_1} + \frac{d}{v_2}$$

and the time difference:

$$\Delta t = t_2 - t_1 = \frac{2h}{v_1} + d\left(\frac{1}{v_2} - \frac{1}{v_1}\right).$$

An interference maximum or minimum of the resultant displacement amplitude at A occurs whenever

$$\cos(2\pi n \Delta t) = \pm 1$$

where n = wave frequency (cps). Again only maxima may be discussed from here on. Hence,

$$\cos 2\pi n \left[\frac{2h}{v_1} + d\left(\frac{1}{v_2} - \frac{1}{v_1}\right)\right] = +1.$$

Let r represent the order number (0, 1, 2, 3-----) then

$$\pm 2\pi n \left[\frac{2h}{v_1} + d\left(\frac{1}{v_2} - \frac{1}{v_1}\right)\right] = 2r\pi$$

or

$$\pm\left[\frac{2h}{v_1} + d\left(\frac{1}{v_2} - \frac{1}{v_1}\right)\right] = \frac{r}{n}. \qquad (16)$$

Two adjacent maxima may occur at the frequencies n_1 and n_2, where $n_2 > n_1$ and have the order numbers r_1 and r_2 with $r_2 = r_1 + 1$.

Call the ratio $\frac{n_1}{n_2} = p$. From eq 16 follows:

$$p = \frac{n_1}{n_2} = \frac{r_1}{r_2} = \frac{r_1}{r_1+1} \qquad (16a)$$

$$pr_1 + p = r_1$$

$$pr_1 - r_1 = -p$$

$$r_1(p-1) = -p$$

$$r_1 = \frac{p}{1-p}. \qquad (17)$$

Eq 17 will be used to determine the order number r from a displacement-frequency graph.

Let $\Delta d = d_2 - d_1$ be the distance between two adjacent maxima, where $d_2 > d_1$.

Consider a constant frequency n.

From eq 16 follows:

$$\pm \left[\frac{2h}{v_1} + d_1 \left(\frac{1}{v_2} - \frac{1}{v_1} \right) \right] = \frac{r}{n}$$

and

$$\pm \left[\frac{2h}{v_1} + d_2 \left(\frac{1}{v_2} - \frac{1}{v_1} \right) \right] = \frac{r+1}{n} \quad .$$

By subtraction:

$$\pm \left[(d_2 - d_1) \left(\frac{1}{v_2} - \frac{1}{v_1} \right) \right] = + \frac{1}{n}$$

$$\Delta d \left(\frac{1}{v_2} - \frac{1}{v_1} \right) = \pm \frac{1}{n}$$

or

$$\frac{1}{v_2} - \frac{1}{v_1} = \pm \frac{1}{n \Delta d} \tag{18}$$

Hence, in case of refraction the distance Δd between two adjacent interference maxima is independent of the distance d between disturbing force and detector. This differs from the previously discussed reflection effect ($d < d^{max} < \frac{4h^2 - \lambda^2}{2}$).

If v_1 and v_2 can be determined experimentally, eq 18 may be used to check magnitude and sign of $\frac{1}{n \Delta d}$.

From eq 16, the depth h of the upper stratum is:

$$h = \frac{v_1}{2} \left[\mp d \left(\frac{1}{v_2} - \frac{1}{v_1} \right) + \frac{r}{n} \right] \tag{19}$$

or by substituting eq 18:

$$h = \frac{v_1}{2} \left[\mp \frac{d}{n \Delta d} + \frac{r}{n} \right] . \tag{20}$$

Since this equation for the depth h includes only the velocity v_1 in the upper stratum, some of the complications connected with the impact method can be avoided. A low-velocity stratum between two high-velocity strata required no special treatment, as is necessary for the impact method (next section, Case III).

It should be kept in mind, however, that two other terms are required. First, the distance Δd between two adjacent interference maxima has to be determined and, second, the order number r must be computed.

Case II. Three strata with higher velocity in each lower bed: To simplify the calculation U-shaped paths are assumed arbitrarily, (Fig. 13), the first path following O-B-C-A and the second path following O-D-E-A, that is $i_1=i_2$.

The traveling times for the wave pencils are:

$$t_1 = \frac{2h_1}{v_1} + \frac{d}{v_2}$$

and

$$t_2 = \frac{2h_1}{v_1} + \frac{2h_2}{v_2} + \frac{d}{v_3}$$

and the time difference:

$$\Delta t = t_2 - t_1 = \frac{2h_2}{v_2} + d\left(\frac{1}{v_3} - \frac{1}{v_2}\right).$$

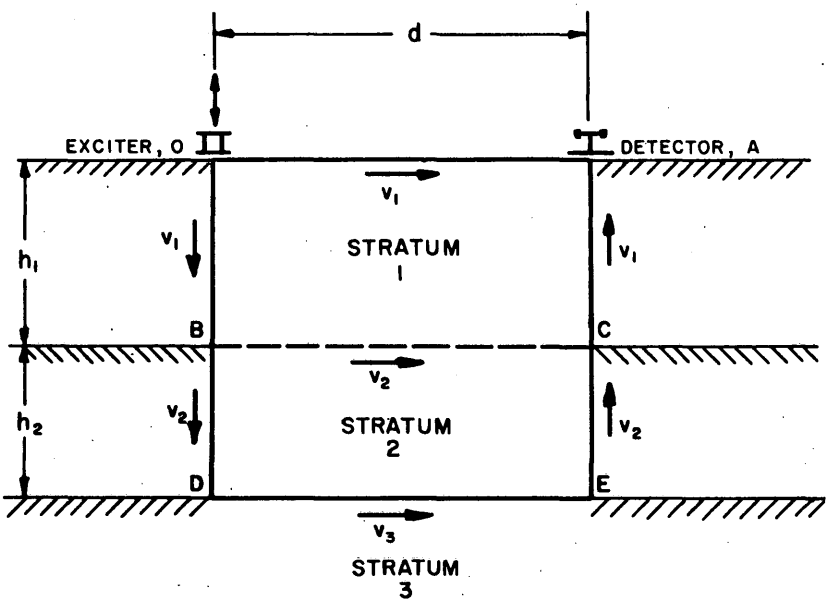

Figure 13. Ray path – three strata – sinusoidal force excitation: refraction.

Interference maxima occur for

$$\pm \frac{2h_2}{v_2} + d\left(\frac{1}{v_3} - \frac{1}{v_2}\right) = \frac{r}{n}$$

and finally

$$h_2 = \frac{v_2}{2}\left(\mp \frac{d}{n\Delta d} + \frac{r}{n}\right) \qquad (21)$$

by applying the same reasoning as in Case I.

Summarizing the results, it may be stated that under certain conditions eq 20 and 21 are valid for strata-depth determinations from time-distance, time-displacement, and frequency-distance graphs obtained experimentally by sinusoidal force excitation.

Impact force excitation

Purpose. To show that impact excitation yields time-distance graphs which can be used to determine reflection and refraction phenomena in stratified soils (Slichter, 1932; Leet, 1938; Bullen, 1947; Jeffreys, 1936; Mattice and Lieber, 1954; Macelwane and Sohon, 1936).

Angle of ray pencils. The direction of reflected and refracted rays depends upon the velocity only and is independent of the type of wave. Snell's law is applicable (Fig. 14):

$$\frac{\sin i_1}{\sin i_2} = \frac{v_1}{v_2}$$

where i_1 = angle of incident ray in the upper stratum with velocity v_1 and i_2 = angle of refracted ray in the lower stratum with velocity v_2.

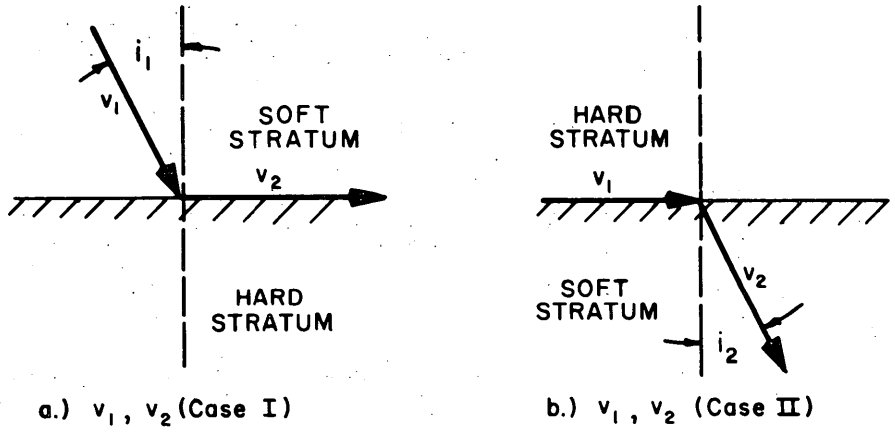

Figure 14. Grazing angles – impact force excitation.

For $i_2 = 90°$ the refracted ray grazes the lower stratum and $v_1 < v_2$ (Case I, Fig. 14a):

$$\sin i_1 = \frac{v_1}{v_2}\ ;\ v_1 = v_2 \sin i_1;\ \tan i_1 = \frac{v_1}{\sqrt{v_2^2 - v_1^2}}\ ;\ \cos i_1 = \frac{\sqrt{v_2^2 - v_1^2}}{v_2}. \quad (22)$$

For $i_1 = 90°$ the incident ray grazes the upper stratum and $v_2 < v_1$ (Case II, Fig. 14b):

$$\sin i_2 = \frac{v_2}{v_1};\ v_2 = v_1 \sin i_2;\ \tan i_2 = \frac{v_2}{\sqrt{v_1^2 - v_2^2}}\ . \quad (23)$$

Three cases will be discussed: first a two-strata formation with $v_1<v_2$, second a three-strata formation with $v_1<v_2<v_3$, and third, a three-strata formation with $v_1>v_2<v_3$.

Case I. A low velocity stratum on a high velocity stratum. Figure 15a represents a distance-time graph with $v_1<v_2$, where A_1 = point of intersection between gradient of v_1 and v_2, and O the starting point for v_1.

Figure 15b is the corresponding wave-front diagram where:

λ_1 = wave length in upper stratum = $\frac{v_1}{n}$

λ_2 = wave length in lower stratum = $\frac{v_2}{n}$

n = excited frequency

i_1 = critical (grazing) angle

h = depth of upper stratum

A_2 = point of equal arrival time for rays with wave length λ_1 and λ_2.

The assumption is made that no possible ray paths exist between O and A.

Figure 15c shows the direct path $OA_3 = d$ along the surface of the upper stratum, and the indirect path O-B-C-A_3 through the upper stratum and grazing the upper surface of the lower stratum.

A_3 is the point of equal arrival time for two rays, one with velocity v_1 and the other with velocities v_1-v_2-v_1.

The position of points A in Fig. 15 a, b, c is one of particular significance.

Let t = travel time for ray O-B-C-A,
t_1 = travel time for ray O-B
t_2 = travel time for ray B-D.

Then $\frac{t}{2} = t_1 + t_2$, where in combination with eq 22:

$$t_1 = \frac{OB}{v_1} = \frac{h}{\cos i_1 v_1} = \frac{h}{\cos i_1 v_2 \sin i_1} = \frac{2h}{v_2 \sin 2i_1}$$

and

$$t_2 = \frac{d/2 - FB}{v_2} = \frac{d/2 - h\tan i_1}{v_2} .$$

Thus

$$\frac{t}{2} = \frac{h}{v_1 \cos i_1} + \frac{d/2 - h\tan i_1}{v_2} . \qquad (24)$$

Substituting the values of eq 22 for $\cos i_1$ and $\tan i_1$ yields:

$$\frac{d}{v_1} = \frac{2h}{v_1} \frac{v_2}{\sqrt{v_2^2 - v_1^2}} + \frac{d}{v_2} - \frac{2h}{v_2} \frac{v_1}{\sqrt{v_2^2 - v_1^2}} \qquad (25)$$

$$\frac{d}{v_1} - \frac{d}{v_2} \frac{2h}{\sqrt{v_2^2 - v_1^2}} \left(\frac{v_2}{v_1} - \frac{v_1}{v_2} \right)$$

or

$$d(v_2 - v_1) = \frac{2h}{\sqrt{v_2^2 - v_1^2}} \quad (v_2^2 - v_1^2)$$

$$d^2(v_2 - v_1)^2 = 4h^2 \, (v_2^2 - v_1^2).$$

and

$$h^2 = \frac{d^2}{4} \frac{(v_2 - v_1)^2}{v_2^2 - v_1^2} = \frac{d^2}{4} \frac{v_2 - v_1}{v_2 + v_1} .$$

Finally:

$$h = \frac{d}{2}\sqrt{\frac{v_2 - v_1}{v_2 + v_1}} . \tag{26}$$

Obviously this equation is valid only for $v_2 > v_1$.

In Figure 15c point E represents the smallest value for distance d where refraction effects can occur. Let the critical distance OE = d_c, then

$$\tan i_1 = \frac{d_c}{2h}$$

or

$$d_c = 2h \tan i_1 \tag{27}$$

This distance d_c coincides with values obtained by Griggs (1956), indicating the source detector distance from where shear waves become predominant. All numerical calculations are confined to the range $d > d_c$.

For checking an experimentally obtained distance-time graph (Fig. 15a) let t_c be the intersection of gradient v_2 with the time axis, that is, a point where d = 0 and $t = t_c$.

Eq 24 changes into:

$$t_c = \frac{2h\, v_2}{v_1\sqrt{v_2^2 - v_1^2}} - \frac{2h}{v_2} \frac{v_1}{\sqrt{v_2^2 - v_1^2}} = \frac{2h}{\sqrt{v_2 - v_1^2}} \left(\frac{v_2}{v_1} - \frac{v_1}{v_2}\right)$$

or

$$t_c^2 = \frac{4h^2}{v_1^2 v_2^2} \quad (v_2^2 - v_1^2)$$

and finally

$$t_c = 2h\sqrt{\frac{v_2^2 - v_1^2}{v_1^2 - v_2^2}} = 2h\sqrt{\frac{1}{v_1^2} - \frac{1}{v_2^2}} . \tag{28}$$

Case II. Three strata with higher velocity in each lower bed. Figure 16 represents a ray path for three beds with $v_3 > v_2 > v_1$. The first path, O-B'-C'-A is identical to the indirect path for a two-layer system, Figure 15c.

The second indirect path O-B-C-H-I-A, is refracted at B into the second bed and grazes at C, the third layer.

A is the point of equal arrival time for the two rays, one with the velocities v_1-v_2-v_1 and the other with velocities v_1-v_2-v_3-v_2-v_1.

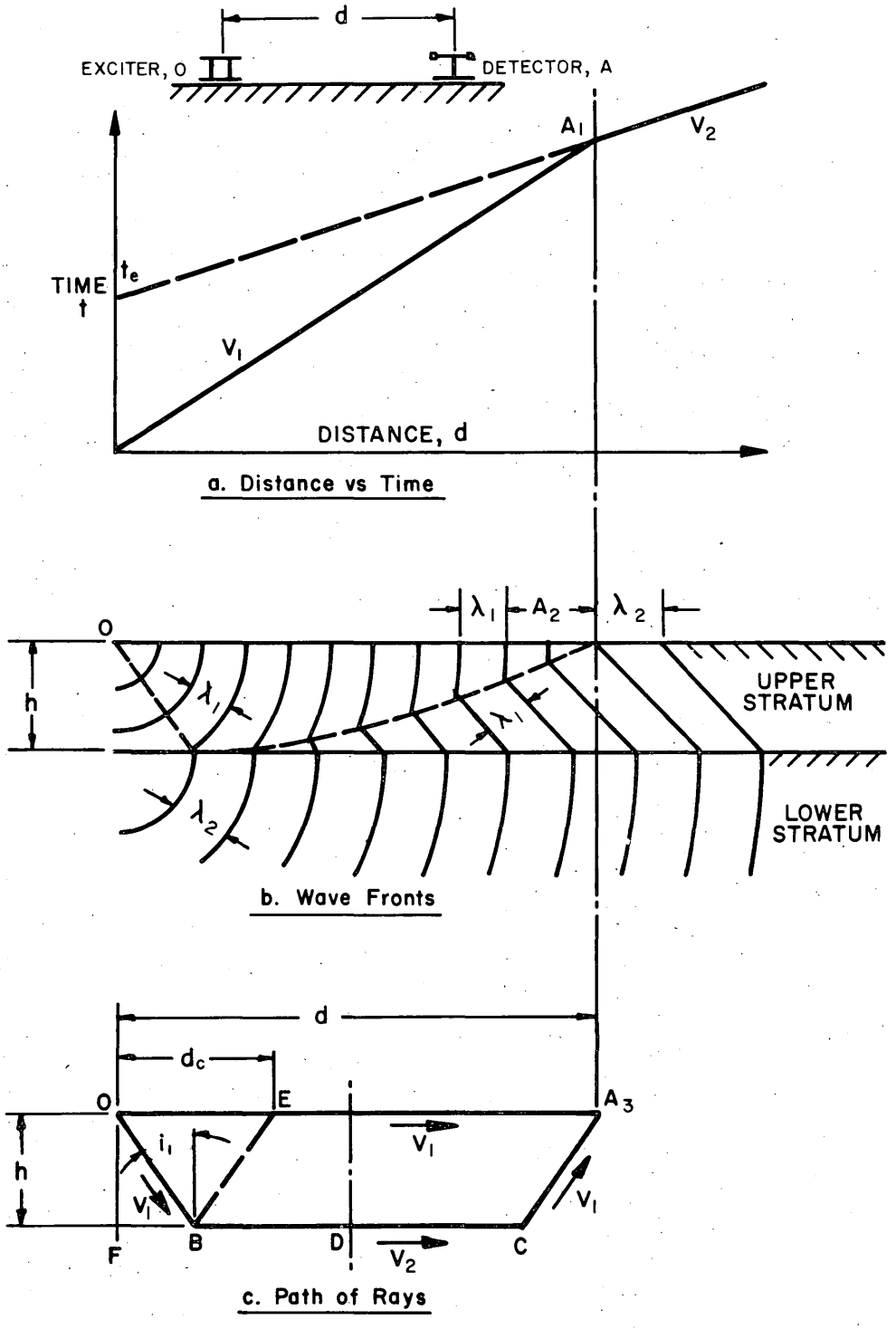

Figure 15. Impact force excitation ($v_1 < v_2$) in two strata.

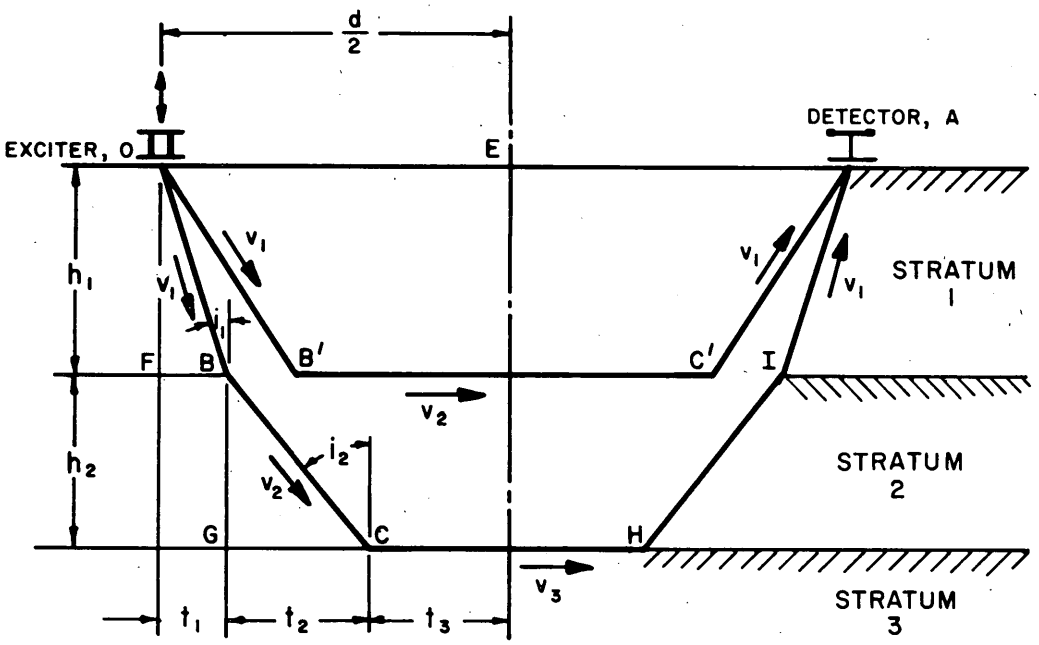

Figure 16. Ray paths with three strata – impact force excitation ($v_1<v_2<v_3$).

Let t = travel time for ray O-B-C-H-J-A

t_1 = travel time for ray O-B

t_2 = travel time for ray B-C

t_3 = travel time for ray C-D.

Then

$$\frac{t}{2} = t_1 + t_2 + t_3 \tag{29}$$

where

$$t_1 = \frac{OB}{v_1}\ ;\ t_2 = \frac{BC}{v_2}\ ;\ t_3 = \frac{CD}{v_3} = \frac{\frac{d}{2} - FB - GC}{v_3}\ .$$

Similar to the previous discussion on refraction:

$$\frac{\sin i_1}{\sin i_2} = \frac{v_1}{v_2}\ ,\ \sin i_2 = \frac{v_2}{v_3}\ \text{ or } \sin i_1 = \sin i_2\ \frac{v_1}{v_2} = \frac{v_2}{v_3}\quad \frac{v_1}{v_2} = \frac{v_1}{v_3}$$

$$\cos i_1 = \frac{\sqrt{v_3^2 - v_1^2}}{v_3}\ ,\ \cos i_2 = \frac{\sqrt{v_3^2 - v_2^2}}{v_3}\ ,\ \tan i_1 = \frac{v_1}{\sqrt{v_3^2 - v_1^2}}\ \text{and}\ \tan i_2 = \frac{v_2}{\sqrt{v_3^2 - v_2^2}}\ .$$

Furthermore, from Figure 16:

$$OB = \frac{h_1}{\cos i_1}\quad BC = \frac{h_2}{\cos i_2}\ ,\quad FB = h_1 \tan i_1 \text{ and } GC = h_2 \tan i_2.$$

Substituting these values into eq 29 yields:

$$\frac{t}{2} = \frac{h_1}{\cos i_1 \, v_1} + \frac{h_2}{\cos i_2 \, v_2} + \frac{\frac{d}{2} - h_1 \tan i_1 - h_2 \tan i_2}{v_3}$$

or

$$\frac{t}{2} = \frac{h_1}{\sqrt{v_3^2 - v_1^2 \frac{v_1}{v_3}}} + \frac{h_2}{\sqrt{v_3^2 - v_2^2 \frac{v_2}{v_3}}} + \frac{d}{2v_3} - \frac{h_1}{v_3} \sqrt{\frac{v_1}{v_3^2 - v_1^2}} - \frac{h_2}{v_3} \sqrt{\frac{v_2}{v_3^2 - v_2^2}} \, . \tag{30}$$

From a combination with eq 25 follows:

$$h_1 \frac{v_2}{v_1} \frac{1}{\sqrt{v_2^2 - v_1^2}} + \frac{d}{2v_2} - h_1 \frac{v_1}{v_2} \frac{1}{\sqrt{v_2^2 - v_1^2}} = \left\{ h_1 \frac{v_3}{v_1} \frac{1}{\sqrt{v_3^2 - v_1^2}} + \right.$$

$$\left. + h_2 \frac{v_3}{v_2} \frac{1}{\sqrt{v_3^2 - v_2^2}} + \frac{d}{2v_3} - h_1 \frac{v_1}{v_3} \frac{1}{\sqrt{v_3^2 - v_1^2}} - h_2 \frac{v_3}{v_3} \frac{1}{\sqrt{v_3^2 - v_2^2}} \right\}$$

or

$$h_2 \left(\frac{v_3}{v_2} \frac{1}{\sqrt{v_3^2 - v_2^2}} - \frac{v_2}{v_3} \frac{1}{\sqrt{v_3^2 - v_2^2}} \right) = \left\{ \frac{d}{2} \left(\frac{1}{v_2} - \frac{1}{v_3} \right) + h_1 \left[\frac{v_2}{v_1} \frac{1}{\sqrt{v_2^2 - v_1^2}} \right. \right.$$

$$\left. \left. - \frac{v_1}{v_2} \frac{1}{\sqrt{v_2^2 - v_1^2}} - \frac{v_3}{v_1} \frac{1}{\sqrt{v_3^2 - v_1^2}} + \frac{v_1}{v_3} \frac{1}{\sqrt{v_3^2 - v_1^2}} \right] \right\}$$

and

$$h_2 = \frac{\frac{d}{2} \left(\frac{1}{v_2} - \frac{1}{v_3} \right) + h_1 \left[\frac{1}{\sqrt{v_2^2 - v_1^2}} \left(\frac{v_2}{v_1} - \frac{v_1}{v_2} \right) - \frac{1}{\sqrt{v_3^2 - v_1^2}} \frac{v_3}{v_1} - \frac{v_1}{v_3} \right]}{\frac{1}{\sqrt{v_3^2 - v_2^2}} \left(\frac{v_3}{v_2} - \frac{v_2}{v_3} \right)} \, .$$

Multiplying by $2v_1v_2v_3$:

$$h_2 = \frac{d v_1 (v_3 - v_2) + 2h_1 \, v_1 \left[\frac{v_2^2 v_3 - v_1^2 v_3}{\sqrt{v_2^2 - v_1^2}} - \frac{v_3^2 v_2 - v_1^2 v_2}{\sqrt{v_3^2 - v_1^2}} \right]}{2 \frac{v_3^2 v_1 - v_2^2 - v_1}{\sqrt{v_3^2 - v_2^2}}}$$

or

$$h_2 = \frac{d v_1 (v_3 - v_2) + 2h_1 \left[v_3 \sqrt{v_2^2 - v_1^2} - v_2 \sqrt{v_3^2 - v_1^2} \right]}{2v_1 \sqrt{v_3^2 - v_2^2}}$$

and finally

$$h_2 = \frac{d v_1 (v_3 - v_2) - 2h_1 \left[v_2 \sqrt{v_3^2 - v_1^2} - v_3 \sqrt{v_2^2 - v_1^2} \right]}{2v_1 \sqrt{v_3^2 - v_2^2}} \, . \tag{31}$$

Case III. A low-velocity stratum between two high-velocity strata. If a hard bed lies above a soft bed a grazing ray on the lower surface of the upper stratum will be refracted into the lower stratum and a gap in the distance-time graph may develop.

Figure 17 indicates that the velocity v_2 in the soft bed can have a maximum and a minimum value:

$$v_2^{max} = \frac{d + \ell}{t^{min}} = v_1 \tag{32}$$

$$v_2^{min} = \frac{d}{t^{max}} < v_1 . \tag{33}$$

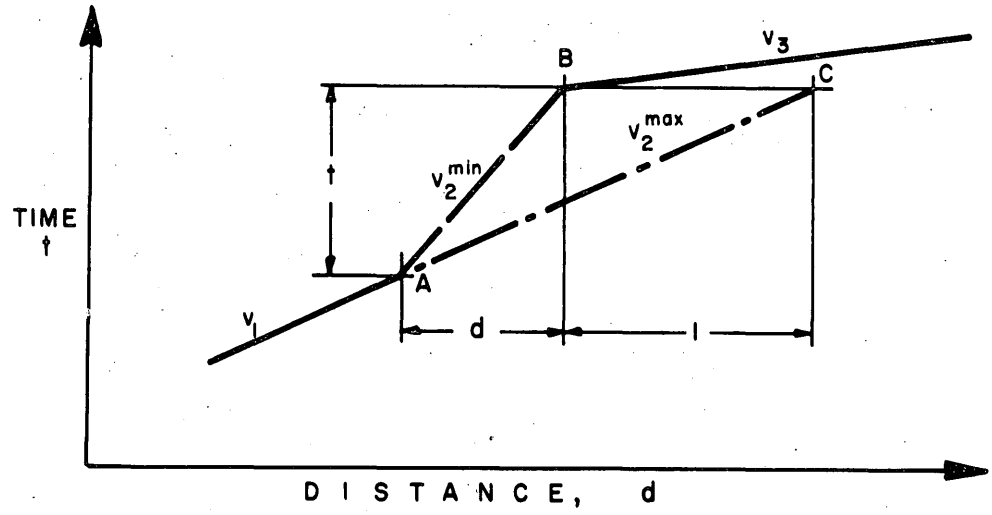

Figure 17. Distance versus time – two strata – impact force excitation ($v_1 > v_2$).

A-B represents the gap in the distance-time graph due to the soft bed. A-C is the extension of the distance-time graph ending at A and defining v_1, and v_3 is the velocity in the lowest bed.

Eq 24 can be rewritten in the form:

$$\frac{t}{2} = \frac{2h}{v_2 \sin 2i_2} + \frac{d/2 - h\tan i_2}{v_2} . \tag{34}$$

Determination of h^{max}: $\frac{t}{2}$ reaches a minimum when the second term on the right side of eq 34 becomes zero; that is, for:

$$\frac{d}{2} = h \tan i_2 \quad \text{or} \quad \tan^2 i_2 = \frac{d^2}{4h^2} .$$

Substituting $\sin 2i_2 = \frac{2 \tan i_2}{1+\tan^2 i_2}$ yields:

$$\frac{t^{min}}{2} = \frac{2h(1+\tan^2 i_2)}{v_2\, 2\tan i_2} = \frac{h\,(1+\frac{d^2}{4h^2})}{v_2\,\frac{d}{2h}} = \frac{4h^2+d^2}{2d\,v_2}$$

or

$$\frac{2h^2}{dv_2} = \frac{t^{min}}{2} - \frac{d}{2v_2}$$

and

$$h^2 = \frac{dv_2}{2}\left(\frac{t^{min}}{2} - \frac{d}{2v_2}\right) = \frac{d}{4}\,(v_2 t^{min} - d).$$

From eq 32 follows: $v_2^{max}\, t^{min} = d+\ell$, where ℓ = BC (Fig. 22) or $\ell = v_2^{max}\, t^{min} - d$.

Thus

$$(h^2)^{max} = \frac{d}{4}\,\ell$$

and finally

$$h^{max} = \frac{1}{2}\sqrt{d\ell}\ . \qquad (35)$$

Determination of h^{min}: Rewriting eq 24 in the form:

$$\frac{h}{v_2 \sin i_2 \cos i_2} - \frac{h \tan i_2}{v_2} = \frac{t}{2} - \frac{d}{2v_2}$$

yields:

$$\frac{h}{v_2}\left(\frac{1}{\sin i_2 \cos i_2} - \frac{\sin i_2}{\cos i_2}\right) = \frac{1}{2}\left(t - \frac{d}{v_2}\right)$$

or

$$\frac{h}{v_2}\ \frac{1-\sin^2 i_2}{\sin i_2 \cos i_2} = \frac{1}{2}\left(t - \frac{d}{v_2}\right)$$

and

$$\frac{h}{v_2}\ \frac{1}{\tan i_2} = \frac{1}{2}\left(t - \frac{d}{v_2}\right)$$

$$h = \frac{1}{2}\, v_2 \tan i_2 \left(t - \frac{d}{v_2}\right) = \frac{\tan i_2}{2}\,(t v_2 - d).$$

From eq 23 and 32 finally:

$$h^{min} = \frac{\ell}{2} \frac{v_2^{min}}{\sqrt{v_1^2 - (v_2^2)^{min}}} . \qquad (36)$$

In this equation, v_1 is the velocity as defined by the gradient of AC and v_2^{min} is the velocity defined by the gradient of AB (Fig. 17), indicating the slowest possible velocity in the soft stratum.

The average value between h^{max} and h^{min}, as determined from eq 35 and 36, will yield the soil depth of a soft bed sandwiched between two hard beds accurately enough for most practical purposes.

Summarizing the results it may be stated that eq 26, 31, 35, and 36 can be used to determine strata depths from time-distance curves experimentally obtained by impact force excitation.

SELECTED BIBLIOGRAPHY

Ahlvin, R.G. (1954) Direct measurements of shear stress in soil mass, Proceedings, Highway Research Board, vol. 33, p. 471-474.

American Society for Testing Materials (1953) Symposium on dynamic testing of soils, Special Technical Publication no. 156.

Bergström, S.G. and Linderholm, S. (1946) A dynamic method for determining average elastic properties of surface soil layers, Swedish Cement and Concrete Research Institute, Royal Technical University, Stockholm, Proceedings N: R7, p. 1-47.

Bernhard, R.K. (1936a) Geophysical study of soil dynamics, American Institute of Mining and Metallurgical Engineers, Technical Publication no. 834, Geophysical Prospecting No. 55 and Transaction, Geophysics, vol. 138, p. 326-349.

_____ (1936b) A practical application of artificial vibrations, Proceedings, Highway Research Board, p. 288-293.

_____ (1949) Study on mechanical oscillators, Proceedings, American Society for Testing Materials, vol. 49, p. 1016-1036.

_____ (1956) On microseismics, American Society for Testing Materials, Special Technical Publication 206, p. 83-102.

_____ (1958) A study on soil wave propagation, Proceedings, Highway Research Board, vol. 37, p. 618-646.

_____ (1961) Biaxial stress fields in noncohesive soils subjected to vibratory loads, American Society for Testing Materials, Symposium on Soil Dynamics. Special Technical Publication no. 305, p. 1-14.

_____ (1963) Shear stress measurements in situ of soils subjected to vibratory loads, U.S. Army Cold Regions Research and Engineering Laboratory (USA CRREL) Technical Report 90.

_____ (1965) Bibliography on soil dynamics, USA CRREL Special Report 89, 111 p.

Biot, M.A. (1956) Theory of elastic waves in a fluid-saturated porous solid, Part I and II, Journal of the Acoustical Society of America, vol. 28, no. 2, p. 168-191.

SELECTED BIBLIOGRAPHY (Cont'd)

Bullen, K.E. (1947) An introduction to the theory of seismology. New York: Cambridge University Press.

Converse, F.J. (1956) Compaction of cohesive soil by low frequency vibration, Proceedings, American Society for Testing Materials.

_____ and Jones, W.F. (1954) Vibration compaction of cohesive soils, Research Report, California Institute of Technology, for U.S. Navy.

_____ (1955) Further studies on vibration compaction of cohesive soils, Research Report, California Institute of Technology, for U.S. Navy.

Converse, F.J.; Hausman, D.A., and Pauw, A. (1952) Vibration compaction of sand, Research Report, California Institute of Technology, for U.S. Navy.

Griggs, P. (1956) Displacement of sinusoidal earth waves radiating from a point source, Rutgers University, Graduate School thesis.

Heinrich, A. (1930) Über die Ausbreitung von Bodenschwingungen in Abhängigkeit von der Beschaffenheit des Baugrundes, Die Bautechnik, Nov. 28, p. 757-761.

Iida, K. (1937) Determination of the elastic constants of superficial soil and base rock at Maru-no-uti, Tokyo, Bulletin, Earthquake Research Institute, Tokyo University, vol. XV, Part III, p. 836.

Ishimoto, M. and Iida, K. (1936, 37) Determination of elastic constants of soils by means of vibration methods. Modulus of rigidity and Poisson's ratio, Bulletin, Earthquake Research Institute, Tokyo University, vol. XIV, p. 632-657, and Part II, vol. XV, p. 67-85.

Jeffreys, H. (1936) On travel times in seismology, Travaux Scientifiques, Series A, no. 14.

Keller, G.V. (1955) Dispersion of seismic waves near a small explosion, Transactions American Geophysical Union, vol. 36, no. 6, p. 1035-1043.

Knopoff, L. (1955) Small three dimensional seismic models, Transactions American Geophysical Union, vol. 36, no. 6, p. 1029-1034.

_____ (1956) The attenuation of compression waves in loessy media, Bulletin of the Seismological Society of America, vol. 46, no. 1, p. 47-56.

Köhler, R.; Ramspeck, A., and Schulze, G.A. (1936, 38) Veröffentlichungen des Instituts der Deutschen Forschungsgesellschaft für Bodenmechanik (DEGEBO), Technische Hochschule, Berlin, no. 4.

Köhler, R., Eigenschwingungen im Boden, Deutsche Ges. -Bodenmechanik (DEGEBO), Springer, no. 4, p. 3-8.

_____ and Ramspeck, A., Die Ausbreitungsgeschwindigkeit elastischer Wellen im Boden, Deutsche Ges. -Bodenmechanik (DEGEBO), Springer, no. 4, p. 9-37.

Lamb, H. (1904) On propagation of tremors over the surface of an elastic solid, Philosophical Transactions, Royal Society (London), Series A, vol. 203, p. 1-42.

SELECTED BIBLIOGRAPHY (Cont'd)

Leet, L. D. (1938) Practical seismology and seismic prospecting. New York: Appleton, Century-Crofts Inc.

Love, A. E. H. (1911) Problems of geodynamics. Cambridge, England: University Press.

Macelwane, J. B. and Sohon, F. W. (1936) Introduction to theoretical seismology, Part I, Geodynamics. New York: John Wiley.

Mattice, H. C. and Lieber, P. (1954) On attenuation of waves produced in visco-elastic materials, Transactions American Geophysical Union, vol. 35, no. 4, p. 613-624.

Nishimura, G. and Takayama, T. (1937) The vibration due to oblique incident waves of a surface stratum adhering closely to the subjacent medium and the properties of its resonance conditions, Bulletin, Earthquake Research Institute, Tokyo University, vol. XV, Part II, p. 394-440.

Ramspeck, A. and Schulze, G. A., The dispersion of elastic waves in soil, Deutsche Ges. Bodenmechanik (DEGEBO), Springer, no. 6, p. 1-28 (text in German).

Rayleigh, J. W. S. (1885) On waves propagated along the surface of an elastic solid, Proceedings, London Mathematical Society, vol. 17.

Sezawa, K. (1928, 29) Propagation of Rayleigh waves having a certain azimuthal distribution of displacement, Proceedings Imp. Acad. (Japan) vol. IV, p. 267-272, and Further studies on Rayleigh waves having some azimuthal distribution, Bulletin of the Earthquake Research Institute, Tokyo University, vol. VI, p. 1-5.

_____ and Kanai, K. (1935) Decay constants of seismic vibrations of a surface layer, Bull. Earthqu. Res. Inst., Tokyo Univ., vol. XII, Part II, p. 251-257.

_____ (1937a) Resonance phenomena and dissipation waves in the stationary vibrations of a semi-infinite body, Bull. Earthqu. Res. Inst., Tokyo Univ., vol. XV, Part I, p. 1-12.

_____ (1937b) Resonance phenomena and dissipation waves in the stationary vibration of the surface of a spherical cavity, Bull. Earthqu. Res. Inst., Tokyo Univ., vol. XV, Part I, p. 13-20.

_____ (1937c) On the free vibrations of a stratified body subjected to vertical surface loads, Bull. Earthqu. Res. Inst., Tokyo Univ., vol. XV, Part II, p. 359-369.

_____ (1937d) The same stationary vibration of an origin accompanying different types of disturbances, Bull. Earthqu. Res. Inst., Tokyo Univ., vol. XV, Part II, p. 370-375.

_____ (1937e) Relation between the thickness of a surface layer and the amplitudes of dispersive Rayleigh waves, Bull. Earthqu. Res. Inst., Tokyo Univ., vol. XV, Part IV, p. 845-859.

Steinbrenner, W. (1934) Tafeln zur Setzungsberechnung, Die Strasse, vol. 1. See also Terzaghi, K. (1947) Theoretical soil mechanics. New York: Wiley.

APPENDIX A: EQUATIONS FOR COMPUTING STRESS COMPONENTS IN PART II.

Derivations of the equations used for the evaluation in part II are presented here in a condensed version to facilitate an understanding of the theoretical background.

This appendix is subdivided into five parts: 1. Shear stresses, 2. Principal stress differences, 3. Principal stress, 4. Maximum shear stresses, and 5. Direction cosines.

The determination of the principal stress differences (part 2) avoids the rather cumbersome solution of a cubic equation for the principal stresses, thus reducing the computational effort substantially.

1. Shear stresses

Let p_i be the stress components in the 1, 2, and 3 directions at a point on a plane in a stressed solid (Fig. A1a), then

$$\left.\begin{aligned} p_1 &= \ell\sigma_1 + m\,\tau_{21} + n\,\tau_{31} \\ p_2 &= \ell\tau_{12} + m\,\sigma_2 + n\,\tau_{32} \\ p_3 &= \ell\tau_{13} + m\,\tau_{23} + n\,\sigma_3 \end{aligned}\right\} \tag{A1}$$

and values $\tau_{12}=\tau_{21}$, $\tau_{13}=\tau_{31}$, $\tau_{23}=\tau_{32}$

and the normal stress

$$\sigma = \ell p_1 + m p_2 + n p_3 . \tag{A2}$$

From eq A1 and A2 follows:

$$\sigma = \ell(\ell\sigma_1 + m\tau_{12} + n\tau_{31}) + m(\ell\tau_{12} + m\sigma_2 + n\tau_{23}) + n(\ell\tau_{13} + m\tau_{23} + n\sigma_3)$$

or

$$\sigma = \ell^2\sigma_1 + m^2\sigma_2 + n^2\sigma_3 + 2\ell m\,\tau_{12} + 2n\ell\,\tau_{13} + 2mn\,\tau_{23} . \tag{A3}$$

Replacing (σ_1, σ_2, σ_3) by principal stresses (s_1, s_2, s_3) for which all shear stresses (τ_{13}, τ_{23}, τ_{31}) are zero:

Eq A1 yields $p_1 = \ell s_1$; $p_2 = m s_2$; $p_3 = n s_3$

Eq A3 yields $\sigma = \ell^2 s_1 + m^2 s_2 + n^2 s_3$. (A4)

The magnitude of the total stress R is

$$R = \sqrt{p_1^2 + p_2^2 + p_3^2} = \sqrt{\ell^2 s_1^2 + m^2 s_2^2 + n^2 s_3^2} \tag{A5}$$

and the magnitude of the shear stress τ is given by:

$$\tau^2 = R^2 - \sigma^2. \tag{A6}$$

Substituting eq A4 and A5 into eq A6,

APPENDIX A

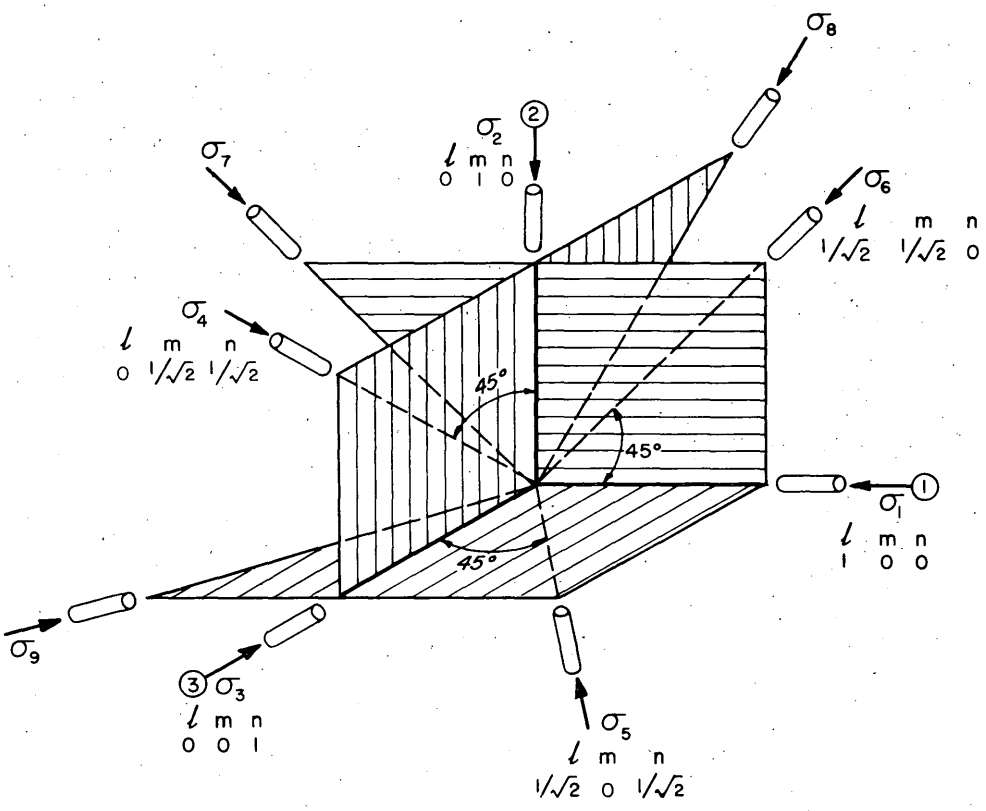

a. Normal Stresses, σ and Direction Cosines, l, m, n

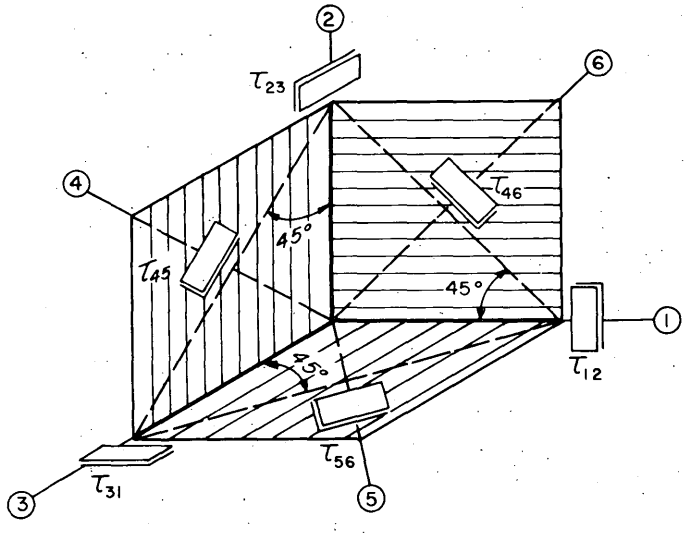

b. Shear Stresses, τ

Figure A1. Notation and measurement systems, three dimensional shear stress experiments.

$$\tau^2 = \ell^2 s_1^2 + m^2 s_2^2 + n^2 s_3^2 - (\ell^2 s_1 + m^2 s_2 + n^2 s_3)^2 \qquad \text{(A7)}$$

or

$$\begin{aligned} \tau^2 = {} & \ell^2 s_1^2 + m^2 s_2^2 + n^2 s_3^2 - \ell^4 s_1^2 - m^4 s_2^2 - n^4 s_3^2 \\ & - 2\ell^2 m^2 s_1 s_2 \quad \text{(a)} \\ & - 2\ell^2 n^2 s_1 s_3 \quad \text{(b)} \\ & - 2m^2 n^2 s_2 s_3 \quad \text{(c)} \end{aligned} \qquad \text{(A8)}$$

Term (a) can be written in the form

$$-2\ell^2 m^2 s_1 s_2 + \ell^2 m^2 s_1^2 + \ell^2 m^2 s_2^2 - \ell^2 m^2 s_1^2 - \ell^2 m^2 s_2^2$$

or

$$\ell^2 m^2 (s_1 - s_2)^2 - \ell^2 m^2 s_1^2 - \ell^2 m^2 s_2^2 \ .$$

Similarly, term (b)

$$\ell^2 n^2 (s_1 - s_3)^2 - \ell^2 n^2 s_1^2 - \ell^2 n^2 s_3^2$$

and term (c)

$$m^2 n^2 (s_2 - s_3)^2 - m^2 n^2 s_2^2 - m^2 n^2 s_3^2 \ .$$

Substituting these values for a, b, c into eq A8:

$$\begin{aligned} \tau^2 = {} & \ell^2 s_1^2 + m^2 s_2^2 + n^2 s_3^2 - \ell^4 s_1^2 - m^4 s_2^2 - n^4 s_3^2 \\ & + \ell^2 m^2 (s_1 - s_2)^2 - \ell^2 m^2 s_1^2 - \ell^2 m^2 s_2^2 \\ & + \ell^2 n^2 (s_1 - s_3)^2 - \ell^2 n^2 s_1^2 - \ell^2 n^2 s_3^2 \\ & + m^2 n^2 (s_2 - s_3)^2 - m^2 n^2 s_2^2 - m^2 n^2 s_3^2 \end{aligned} \qquad \text{(A9)}$$

or

$$\tau^2 = \ell^2 m^2 (s_1 - s_2)^2 + \ell^2 n^2 (s_1 - s_3)^2 + m^2 n^2 (s_2 - s_3)^2 + \ell^2 s_1^2 (1 - \ell^2 - m^2 - n^2) + m^2 s_2^2 (1 - m^2 - \ell^2 - n^2) + n^2 s_3^2 (1 - n^2 - \ell^2 - m^2)$$

and since $\ell^2 + m^2 + n^2 = 1$ (A10)

$$\tau^2 = \ell^2 m^2 (s_1 - s_2)^2 + \ell^2 n^2 (s_1 - s_3)^2 + m^2 n^2 (s_2 - s_3)^2 \qquad \text{(A11)}$$

$$= \ell^2 m^2 (s_1 - s_2)^2 + m^2 n^2 (s_2 - s_3)^2 + n^2 \ell^2 (s_3 - s_1)^2 . \qquad \text{(A11a)}$$

2. Principal stress differences

Substituting into eq A1 the value $p_1 = \ell s$ and $p_2 = ms$,

$$\ell s = \ell \sigma_1 + m \tau_{12} + n \tau_{31}$$

and

$$ms = \ell \tau_{12} + m \sigma_2 + n \tau_{23} \ .$$

In the plane (1-2) $\tau_{31} = \tau_{23} = 0$

or

$$s = \frac{\ell\sigma_1 + m\tau_{12}}{\ell} = \frac{\ell\tau_{12} + m\tau_2}{m}$$

$$\sigma_1 \ell m + m^2 \tau_{12} = \sigma_2 \ell m + \tau_{12}\ell^2$$

$$\ell m (\sigma_1 - \sigma_2) - (\ell^2 - m^2)\tau_{12} = 0 .$$

For $\ell = \cos\theta$ and $m = \sin\theta$

$$(\sigma_1 - \sigma_2) \sin\theta \cos\theta - \tau_{12} (\cos^2\theta - \sin^2\theta) = 0$$

or

$$\frac{\tau_{12}}{\sigma_1 - \sigma_2} = \frac{\sin\theta \cos\theta}{\cos^2\theta - \sin^2\theta} = \tfrac{1}{2}\tan(2\theta)$$

$$\left.\begin{aligned} \tan(2\theta) &= \frac{\tau_{12}}{\frac{1}{2}(\sigma_1 - \sigma_2)} \\ \text{similarly} \\ \tan(2\phi) &= \frac{\tau_{23}}{\frac{1}{2}(\sigma_2 - \sigma_3)} \\ \text{and} \\ \tan(2\psi) &= \frac{\tau_{13}}{\frac{1}{2}(\sigma_1 - \sigma_3)} . \end{aligned}\right\} \quad \text{(A12)}$$

The angle θ is in plane 1-2, for which

$\ell = \cos\theta$; $m = \sin\theta$, $n = 0$

and eq 11 yields

$$\tau^2 = (s_1 - s_2)^2 \ell^2 m^2 = (s_1 - s_2) \cos^2\theta \sin^2\theta . \quad \text{(A13)}$$

Since $\sin^2\theta \cos^2\theta = \frac{1}{4}\sin^2(2\theta)$, eq 13 changes into

$$\tau^2 = \tfrac{1}{4}(s_1 - s_2)^2 \sin^2 2\theta$$

or

$$\left.\begin{aligned} \sin(2\theta) &= \frac{\tau_{12}}{\frac{1}{2}(s_1 - s_2)} \\ \text{Similarly} \\ \sin(2\phi) &= \frac{\tau_{23}}{\frac{1}{2}(s_2 - s_3)} \\ \text{and} \\ \sin(2\psi) &= \frac{\tau_{13}}{\frac{1}{2}(s_3 - s_1)} . \end{aligned}\right\} \quad \text{(A14)}$$

The ratio of eq A14 to eq A12 yields:

$$\frac{\sin 2\theta}{\tan 2\theta} = \cos 2\theta = \frac{\frac{1}{2}(\sigma_1 - \sigma_2)}{\frac{1}{2}(s_1 - s_2)}$$

and

$$\sin^2(2\theta) + \cos^2(2\theta) = \frac{\tau_{12}^2}{[\frac{1}{2}(s_1 - s_2)]^2} + \frac{[\frac{1}{2}(\sigma_1 - \sigma_2)]^2}{[\frac{1}{2}(s_1 - s_2)]^2} = 1$$

$$\tau_{12}^2 + [\tfrac{1}{2}(\sigma_1 - \sigma_2)]^2 = [\tfrac{1}{2}(s_1 - s_2)]^2$$

or

$$\left.\begin{aligned} s_1 - s_2 &= \sqrt{(\sigma_1 - \sigma_2)^2 + 4\tau_{12}^2} \\ \text{similarly} \\ s_1 - s_3 &= \sqrt{(\sigma_1 - \sigma_3)^2 + 4\tau_{13}^2} \\ \text{and} \\ s_2 - s_3 &= \sqrt{(\sigma_1 - \sigma_3)^2 + 4\tau_{23}^2} \end{aligned}\right\} \quad \text{(A15)}$$

3. Principal stresses

From the principal stress differences

$$s_1 - s_3,\ s_1 - s_2,\ \text{and}\ s_2 - s_3$$

and the invariants

$$\sigma_1 + \sigma_2 + \sigma_3 = s_1 + s_2 + s_3$$

follows

$$\left.\begin{aligned} s_1 &= \tfrac{1}{3}[(\sigma_1 + \sigma_2 + \sigma_3) + (s_1 - s_3) + (s_1 - s_2)] \\ s_2 &= s_1 - (s_1 - s_2) \\ s_3 &= s_1 - (s_1 - s_3) \end{aligned}\right\} \quad \text{(A16)}$$

4. Maximum shear stresses

For the maximum shear stresses (s^S): $\ell = m = \pm\frac{1}{2}\sqrt{2}$ or $\ell^2 m^2 = \frac{1}{4}$ and from eq 11

$$(s_{12}^S)^2 = \tfrac{1}{4}(s_1 - s_2)^2$$

or

$$s_{12}^{s} = \tfrac{1}{2}(s_1 - s_2)$$

similarly

$$s_{13}^{s} = \tfrac{1}{2}(s_1 - s_3)$$

and

$$s_{23}^{s} = \tfrac{1}{2}(s_2 - s_3) \qquad \text{(A17)}$$

5. Direction Cosines

Combining eq A5 and A6 yields

$$\tau^2 = \ell^2 s_1^2 + m^2 s_2^2 + n^2 s_3^2 - \sigma^2.$$

Substituting from eq A10:

$$m^2 = 1 - \ell^2 - n^2 \qquad \text{(A18)}$$

$$\tau^2 = \ell^2 s_1^2 + (1 - \ell^2 - n^2) s_2^2 + n^2 s_3^2 - \sigma^2$$

or

$$\tau^2 = \ell^2 s_1^2 + s_2^2 - \ell^2 s_2^2 + n^2 (s_3^2 - s_2^2) - \sigma^2$$

and

$$n^2 = \frac{-\ell^2 s_1^2 - s_2^2 + \ell^2 s_2^2 + \tau^2 + \sigma^2}{s_3^2 - s_2^2} \qquad \text{(A19)}$$

Combining eq A4 and A18 yields:

$$\sigma = \ell^2 s_1 + (1 - \ell^2 - n^2) s_2 + n^2 s_3$$

or

$$\sigma = \ell^2 s_1 + s_2 - s_2 \ell^2 + n^2 (s_3 - s_2) \qquad \text{(A20)}$$

Replacing n from eq A20:

$$\sigma = \ell^2 (s_1 - s_2) + s_2 + \frac{-\ell^2 s_1^2 + \ell^2 s_2^2 - s_2^2 + \tau^2 + \sigma^2}{s_3^2 - s_2^2} (s_3 - s_2)$$

or

$$\sigma = \ell^2 (s_1 - s_2) + s_2 + \frac{\ell^2 (s_2^2 - s_1^2) - s_2^2 + \tau^2 + \sigma^2}{s_3 + s_2}$$

$$\ell = [(s_1 - s_2)(s_3 + s_2) + (s_2^2 - s_1^2)] = \sigma (s_3 + s_2) - s_2 (s_3 + s_2) + s_2^2 - \tau^2 - \sigma^2$$

$$\ell^2 = \frac{\sigma s_3 - s_3 s_2 + s_2 \sigma - s_2^2 + s_2^2 - \sigma^2 - \tau^2}{s_1 s_3 + s_1 s_2 - s_2 s_3 - s_2^2 + s_2^2 - s_1^2}$$

$$\ell^2 = \frac{s_2 s_3 - s_2 \sigma - \sigma s_3 + s_1^2 + \tau^2}{s_2 s_3 - s_2 s_1 - s_1 s_2 + s_1^2}$$

and finally:

$$\left.\begin{aligned} \ell &= \sqrt{\frac{(s_2 - \sigma)(s_3 - \sigma) + \tau^2}{(s_2 - s_1)(s_3 - s_1)}} \\ \text{similarly} \\ m &= \sqrt{\frac{(s_3 - \sigma)(s_1 - \sigma) + \tau^2}{(s_3 - s_2)(s_1 - s_2)}} \\ \text{or} \\ n &= \sqrt{\frac{(s_1 - \sigma)(s_2 - \sigma) + \tau^2}{(s_1 - s_3)(s_2 - s_3)}} \quad . \end{aligned}\right\} \tag{A21}$$

Check for invariant I_i

$$I_1 = s_1 + s_2 + s_3 = \sigma_1 + \sigma_2 + \sigma_3 \tag{A22}$$

$$I_2 = + (\sigma_2\sigma_3 + \sigma_1\sigma_3 + \sigma_1\sigma_2 - \tau_{23}^2 - \tau_{12}^2 - \tau_{13}^2) \tag{A23}$$

$$I_3 = + (\sigma_1\sigma_2\sigma_3 - \sigma_1\tau_{13}^2 - \sigma_3\tau_{12}^2 + 2\tau_{12}\tau_{13}\tau_{23}) \tag{A24}$$

Check for direction cosines

From

$$\ell_i + m_i + n_i = \frac{A_i}{\sqrt{A_i^2 + B_i^2 + C_i^2}} + \frac{B_i}{\sqrt{A_i^2 + B_i^2 + C_i^2}} + \frac{C_i}{\sqrt{A_i^2 + B_i^2 + C_i^2}}$$

or

$$\ell^2 + m_i^2 + n_i^2 = \frac{A_i^2 + B_i^2 + C_i^2}{A_i^2 + B_i^2 + C_i^2} = 1 \tag{A25}$$

similarly

$$\Sigma \ell_i^2 = \Sigma m_i^2 = \Sigma n_i^2 = 1 \tag{A26}$$

Check for orthogonality of s_{ii}

$$\left.\begin{aligned} \ell_1\ell_2 + m_1m_2 + n_1n_2 &= 0 \\ \ell_1\ell_3 + m_1m_3 + n_1n_3 &= 0 \\ \ell_2\ell_3 + m_2m_3 + n_2n_3 &= 0 \end{aligned}\right\} \tag{A27}$$

or

$$\left.\begin{aligned} \ell_1 m_1 + \ell_2 m_2 + \ell_3 m_3 &= 0 \\ \ell_1 n_1 + \ell_2 n_2 + \ell_3 n_3 &= 0 \\ m_1 n_1 + m_2 n_2 + m_3 n_3 &= 0 \end{aligned}\right\} \tag{A28}$$

APPENDIX B: EQUATIONS FOR COMPUTER PROGRAM IN PART III.

NOTATION

σ_i	measured normal stresses
τ_{ij}	computed shear stresses
S_i	computed principal stresses
ℓ_i, m_i, n_i	direction cosines
(n)	measuring points
$A_1 - A_2$	reference axis on contact plate
$B_1 - B_2$	"
$C_1 - C_2$	"
I_i	invariant
A_i	cofactors of stress determinant
B_i	"
C_i	"
D_i	$(A_i^2 + B_i^2 + C_i^2)^{1/2}$
λ	eigenvalue of stress matrix
V	eigenvector

With the Cartesian stress components at a point known, the principal stresses are computed from the cubic equation

$$S^3 - I_1 S^2 + I_2 S - I_3 = 0$$

where I_i represents the invariants.

The principal directions corresponding to a particular principal stress are found by using the above equation in its determinant form.

$$\begin{vmatrix} \sigma_x - S_i & \tau_{xy} & \tau_{xz} \\ \tau_{yx} & \sigma_y - S_i & \tau_{yz} \\ \tau_{zx} & \tau_{zy} & \sigma_z - S_i \end{vmatrix} = 0$$

The direction cosines are

$$\ell_i = \frac{A_i}{D_i} \quad m_i = \frac{B_i}{D_i} \quad n_i = \frac{C_i}{D_i}$$

where A_i, B_i and C_i are the co-factors of the stress determinant and $D_i = (A_i^2 + B_i^2 + C_i^2)^{1/2}$.

Greenstadt* describes the Jacobi method of reducing a real symmetric matrix to a diagonal form by a series of plane rotations.

For the 3x3 square symmetrical stress matrix, the problem to be solved is to find a number λ and a vector V such that $AV = \lambda V$, where each λ is an eigenvalue of the matrix A and each related three-dimensional vector, V, is an eigenvector corresponding to the eigenvalue.

An IBM program based upon this method was applied to facilitate the determination of the numerous eigenvalues and eigenvectors.

A basic 1620 digital computer with a 1622 card read-punch was employed.

For each point, values were entered on cards in the following manner:

1. The first card indicated matrix size and degree of precision required.
2. The six succeeding cards represented each matrix element and its numerical value.
3. A final card provided for correcting errors in the punched data through typewriter entries.

Output cards were punched and typewritten records were automatically prepared.

The actual running time for each set of eigenvalues was about five minutes.

* Determination of the characteristic roots of a matrix by the Jacobi method, by John Greenstadt, International Business Machines Corporation. See also

Eigenvalues of real symmetric matrices on the 1620 data processing system, International Business Machines Corporation, and

Mathematical methods for digital computers, by A. Ralston and H. Wilf, ed. John Wiley and Sons.

Stress distribution in non-cohesive soil under vibratory loads, NST-G-15065; by R.K. Bernhard and W.J. Brown.

Unclassified

Security Classification

DOCUMENT CONTROL DATA - R&D

(Security classification of title, body of abstract and indexing annotation must be entered when the overall report is classified)

1. ORIGINATING ACTIVITY *(Corporate author)*
U. S. Army Cold Regions Research and Engineering Laboratory, Hanover, N.H.

2a. REPORT SECURITY CLASSIFICATION
Unclassified

2b. GROUP

3. REPORT TITLE
STRESS AND WAVE PATTERNS IN SOILS SUBJECTED TO DYNAMIC LOADS

4. DESCRIPTIVE NOTES *(Type of report and inclusive dates)*
Research Report

5. AUTHOR(S) *(Last name, first name, initial)*
Bernhard, R. K.

6. REPORT DATE	7a. TOTAL NO. OF PAGES	7b. NO. OF REFS
March 1967	57	44

8a. CONTRACT OR GRANT NO.

b. PROJECT NO.

c. DA Task 1VO25001A13001

d.

9a. ORIGINATOR'S REPORT NUMBER(S)
Research Report 120

9b. OTHER REPORT NO(S) *(Any other numbers that may be assigned this report)*

10. AVAILABILITY/LIMITATION NOTICES
Distribution of this document is unlimited

11. SUPPLEMENTARY NOTES

12. SPONSORING MILITARY ACTIVITY
U. S. Army Cold Regions Research and Engineering Laboratory

13. ABSTRACT

The report is divided into four parts: Parts I and II cover investigations of the reliability of shear stress measurements in soils subjected to vibratory loads for biaxial and triaxial systems, respectively. Part I is a summary only (See SIP 21834 for detailed treatment). Part III is a study of three-dimensional "principal" stress patterns produced in soil subjected to vibratory loads. Part IV is a theoretical analysis of some aspects of soil wave propagation in stratified soil. From the measurements of five shear stresses and one normal stress, the stress distribution of a triaxial system can be determined. In noncohesive soils triaxial stress fields due to vibratory loads can be determined by recording six independent stress components. Sinusoidal force excitation and impact excitation yield time-distance graphs which can be used to determine reflection and refraction techniques in stratified soils.

DD FORM 1 JAN 64 1473

Unclassified

Security Classification

14. KEY WORDS	LINK A		LINK B		LINK C	
	ROLE	WT	ROLE	WT	ROLE	WT
Soils--Wave transmission Soils--Mechanical properties--Testing equipment Soils--Stresses Soils--Properties--Measurement						

INSTRUCTIONS

1. ORIGINATING ACTIVITY: Enter the name and address of the contractor, subcontractor, grantee, Department of Defense activity or other organization *(corporate author)* issuing the report.

2*a*. REPORT SECURITY CLASSIFICATION: Enter the overall security classification of the report. Indicate whether "Restricted Data" is included. Marking is to be in accordance with appropriate security regulations.

2*b*. GROUP: Automatic downgrading is specified in DoD Directive 5200.10 and Armed Forces Industrial Manual. Enter the group number. Also, when applicable, show that optional markings have been used for Group 3 and Group 4 as authorized.

3. REPORT TITLE: Enter the complete report title in all capital letters. Titles in all cases should be unclassified. If a meaningful title cannot be selected without classification, show title classification in all capitals in parenthesis immediately following the title.

4. DESCRIPTIVE NOTES: If appropriate, enter the type of report, e.g., interim, progress, summary, annual, or final. Give the inclusive dates when a specific reporting period is covered.

5. AUTHOR(S): Enter the name(s) of author(s) as shown on or in the report. Enter last name, first name, middle initial. If military, show rank and branch of service. The name of the principal author is an absolute minimum requirement.

6. REPORT DATE: Enter the date of the report as day, month, year; or month, year. If more than one date appears on the report, use date of publication.

7*a*. TOTAL NUMBER OF PAGES: The total page count should follow normal pagination procedures, i.e., enter the number of pages containing information.

7*b*. NUMBER OF REFERENCES: Enter the total number of references cited in the report.

8*a*. CONTRACT OR GRANT NUMBER: If appropriate, enter the applicable number of the contract or grant under which the report was written.

8*b*, 8*c*, & 8*d*. PROJECT NUMBER: Enter the appropriate military department identification, such as project number, subproject number, system numbers, task number, etc.

9*a*. ORIGINATOR'S REPORT NUMBER(S): Enter the official report number by which the document will be identified and controlled by the originating activity. This number must be unique to this report.

9*b*. OTHER REPORT NUMBER(S): If the report has been assigned any other report numbers *(either by the originator or by the sponsor)*, also enter this number(s).

10. AVAILABILITY/LIMITATION NOTICES: Enter any limitations on further dissemination of the report, other than those imposed by security classification, using standard statements such as:

(1) "Qualified requesters may obtain copies of this report from DDC."

(2) "Foreign announcement and dissemination of this report by DDC is not authorized."

(3) "U. S. Government agencies may obtain copies of this report directly from DDC. Other qualified DDC users shall request through _____."

(4) "U. S. military agencies may obtain copies of this report directly from DDC. Other qualified users shall request through _____."

(5) "All distribution of this report is controlled. Qualified DDC users shall request through _____."

If the report has been furnished to the Office of Technical Services, Department of Commerce, for sale to the public, indicate this fact and enter the price, if known.

11. SUPPLEMENTARY NOTES: Use for additional explanatory notes.

12. SPONSORING MILITARY ACTIVITY: Enter the name of the departmental project office or laboratory sponsoring *(paying for)* the research and development. Include address.

13. ABSTRACT: Enter an abstract giving a brief and factual summary of the document indicative of the report, even though it may also appear elsewhere in the body of the technical report. If additional space is required, a continuation sheet shall be attached.

It is highly desirable that the abstract of classified reports be unclassified. Each paragraph of the abstract shall end with an indication of the military security classification of the information in the paragraph, represented as *(TS), (S), (C), or (U)*.

There is no limitation on the length of the abstract. However, the suggested length is from 150 to 225 words.

14. KEY WORDS: Key words are technically meaningful terms or short phrases that characterize a report and may be used as index entries for cataloging the report. Key words must be selected so that no security classification is required. Identifiers, such as equipment model designation, trade name, military project code name, geographic location, may be used as key words but will be followed by an indication of technical context. The assignment of links, rules, and weights is optional.